Prediction & optimization of alkali-activated concrete based on the random forest machine learning algorithm

Sun, Yubo; Cheng, Hao; Zhang, Shizhe; Mohan, Manu K.; Ye, Guang; De Schutter, Geert

DOI
10.1016/j.conbuildmat.2023.131519

Publication date
2023

Document Version
Final published version

Published in
Construction and Building Materials

Citation (APA)
Sun, Y., Cheng, H., Zhang, S., Mohan, M. K., Ye, G., & De Schutter, G. (2023). Prediction & optimization of alkali-activated concrete based on the random forest machine learning algorithm. *Construction and Building Materials*, *385*, Article 131519. https://doi.org/10.1016/j.conbuildmat.2023.131519

Construction and Building Materials 385 (2023) 131519

Contents lists available at ScienceDirect

Construction and Building Materials

journal homepage: www.elsevier.com/locate/conbuildmat

Prediction & optimization of alkali-activated concrete based on the random forest machine learning algorithm

Yubo Sun [a], Hao Cheng [b], Shizhe Zhang [c], Manu K. Mohan [a], Guang Ye [a,c], Geert De Schutter [a,*]

[a] Magnel-Vandepitte Laboratory, Department of Structural Engineering and Building Materials, Ghent University, 9052 Ghent, Belgium
[b] Department of Engineering Structures, Faculty of Civil Engineering and Geosciences, Delft University of Technology, Stevinweg 1, 2628 CN Delft, The Netherlands
[c] Microlab, Section of Materials and Environment, Faculty of Civil Engineering and Geosciences, Delft University of Technology, Stevinweg 1, 2628 CN Delft, The Netherlands

ARTICLE INFO

Keywords:
Alkali-activated concrete
Mix design
Machine learning
Random forest
Prediction
Optimization

ABSTRACT

Alkali-activated concrete (AAC) is regarded as a promising alternative construction material to reduce the CO_2 emission induced by Portland cement (PC) concrete. Due to the diversity in raw materials and complexity of reaction mechanisms, a commonly applied design code is still absent to date. This study attempts to directly correlate the AAC mix design parameters to their performances through an artificial intelligence approach. To be specific, 145 fresh property data and 193 mechanical strength data were collected from laboratory tests on 52 AAC mixtures, which were used as inputs for the machine learning algorithm. Five independent random forest (RF) models were established, which are able to predict fresh and hardened properties (in terms of compressive strength, slump values, static/dynamic yield stress, and plastic viscosity) of AAC with equivalent accuracy reported in the literature. Moreover, an inverse optimization was performed on the RF model obtained to reduce the sodium silicate dosages, which may further mitigate the environmental impact of producing AAC. The present RF model gives practical information on AAC mix design cases.

1. Introduction

Concrete is the most used construction material in view of the advantages in availability, cost, and many other aspects [1]. However, the growing demand for concrete brings great environmental impact due to rapid urbanization in recent years, and it has become a major concern worldwide. As the primary binder applied in concrete materials, the production of Portland cement (PC) is accompanied with heavy energy consumptions. It has been reported that the PC clinker production accounted for 5–8% of global CO_2 emissions [2], causing intense pressure to meet carbon–neutral by 2050.

Alkali-activated material (AAMs), which was developed as a low-carbon binder, has been regarded as one of the most promising alternatives to replace PC materials in concrete. Instead of the hydration in PC materials, the alkali-activation reaction takes place due to the continuous dissolution of aluminosilicate precursors in alkaline media [3]. The dissolved Al and Si tetrahedrons are connected to each other as the backbone through polymerizations, and further incorporated with the alkali/alkali-earth cations to reassemble highly ordered structures [4,5,6]. It is indicated that the microstructure of reaction products is greatly dependent on the availability of calcium content in the precursors [7].

In reality, however, precursors are insufficiently reactive, in particular those derived from different waste streams. In that case, alkaline activators are applied to promote the dissolution [8], which introduces more complex interactions into the AAM system as compared to PC materials. With the intention to make use of industrial wastes and by-products as much as possible, various types of precursors and alkaline substances could be utilized in AAMs. The diversity of raw materials may provide numerous possible mixture combinations. However, variations in material properties on the other hand pose great challenges towards developing a standardized design code, and more insights into the reaction mechanisms are needed to provide desirable AAM mix designs in a predictable and reliable way [9]. Even though there exist several types of commercialized alkali-activated concrete (AAC) products in many regions of the world, the construction with AAC is still limited to a few demonstration structures due to the lack of mature design regulations [10]. In practical applications, parallel PC concretes are recommended to be tested as a reference in the existing design codes dedicated for AAC (the Australian guideline CIA Z16-2011 and the

* Corresponding author.
geert.deschutter@ugent.be ()

https://doi.org/10.1016/j.conbuildmat.2023.131519
Received 16 March 2023; Received in revised form 17 April 2023; Accepted 20 April 2023
Available online 27 April 2023

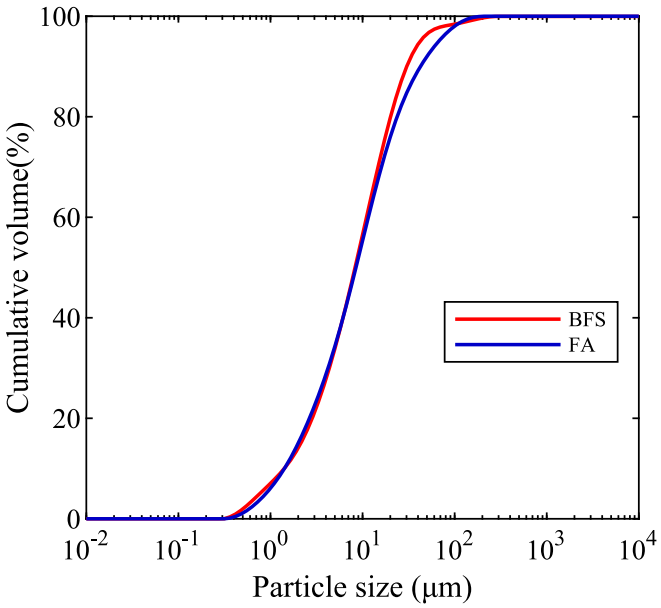

Fig. 1. Particle size distribution curves of precursors.

British standard PAS 8820:2016), through which at least an equivalent performance to meet the requirement of PC concrete can be ensured. Whilst such procedures might lead to extensive extra workloads in the pre-design phase to produce AACs.

With the development of machine learning (ML) algorithms, an artificial intelligence (AI) approach is established to capture the features of diverse and complex systems [11,12]. Previous studies have well-illustrated the feasibility of predicting the performances of PC concretes by using ML algorithms, including artificial neural network (ANN), random forest (RF), support vectors machine (SVM), gradient boosting (GB), etc. [13,14,15,16,17,18,19]. Considering the diversity and complexity of AACs, the development of ML algorithms has created a shortcut for making performance predictions based on the data collected from experiments [20,21,22,23]. It is noticed that the majority of existing AAC models focus more on mechanical properties. For instance, Ramagiri et al. [24] compared the accuracy of 5 RF models with different configurations to predict the strength of AAC concrete. Toufigh and Jafari [25] proposed a prediction model to estimate the compressive strength of fly ash (FA)-based AAC out of the 162 mixtures collected from the papers published. Peng and Unluer [26] achieved ± 20% accuracy to predict the compressive strength of FA-based AAC, which was done through ANN, SVM, and extreme learning machine (ELM) algorithms. Gomaa et al. [27] performed numerous experiments to derive predictive models for compressive strength and initial slump flow of AAC (made of class C fly ashes). Nevertheless, the relevant data and models on the workability and rheological behaviors of AAC are still very limited.

In this research, results of lab tests on 52 AAC mixtures (193 and 145 data of strength and fresh properties, respectively) were collected as input. Five RF models are established for predicting the fresh and hardened behaviors of AAC (in terms of compressive strength, slump values, and rheological parameters). Moreover, an inverse application has been proposed based on the RF model, which assists to optimize the mix design parameter and further reduces the environmental impact of AAC. The regression models developed may provide guidance information on the mix design of AAC, while the strength and fresh properties collected can be served as a supplement to expand the current AAC database.

2. Methodology

2.1. Materials

In this study, ground granulated blast furnace slag (BFS) and coal fly ash (FA) were used as precursors to prepare the AAC. BFS was provided by Ecocem Benelux B.V., with a density of 2890 kg/m^3, and FA (Class F, 2300 ± 200 kg/m^3) was produced as type II filler in cementitious materials according to NEN-EN 450–1: 2012 by Vliegasunie B.V.. The particle size distribution of precursors was measured by laser diffraction, as shown in Fig. 1. It's been observed that BFS and FA have very similar particle sizes, with d_{50} values of 8.28 and 8,48 μm, respectively. The particle morphology of precursor grains was observed with a scanning electron microscope (SEM), as shown in Fig. 2. BFS showed angular particles with irregular shapes, while spherical particles have been observed in FA samples. Furthermore, their compositions were determined by X-ray fluorescence (XRF) and loss on ignition (LOI), as presented in Table 1.

Sodium hydroxide and sodium silicate were used to prepare the alkaline activators in this study. Reagent-grade sodium hydroxide anhydrous pearls (>99 %) were provided by Brenntag N.V., and the sodium silicate solution (15% Na_2O, 30% SiO_2, and 55% water) was

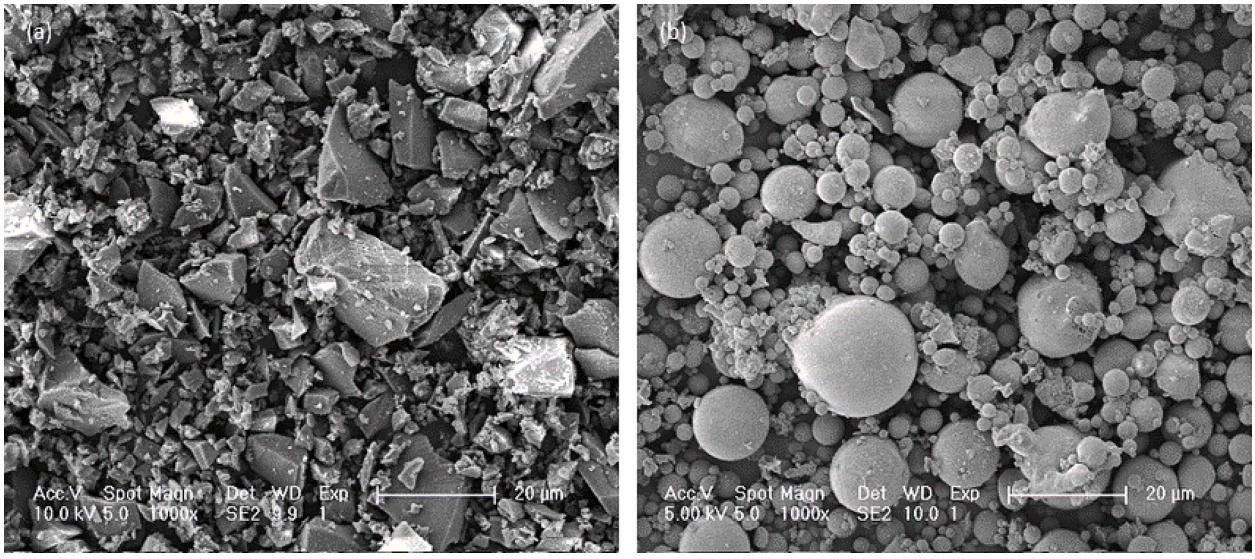

Fig. 2. Morphology by SEM (1000 × magnification) (a) BFS particles; (b) FA particles.

Table 1
Chemical composition of BFS/FA measured by XRF and LOI (mass %).

Precursor	CaO	SiO_2	Al_2O_3	MgO	SO_3	TiO_2	K_2O	Fe_2O_3	MnO	ZrO_2	Other	LOI [a]
BFS	40.9	31.1	13.7	9.16	2.31	1.26	0.69	0.40	0.31	0.12	0.05	0.10
FA	3.74	56.7	24.0	1.75	1.04	1.16	2.30	6.34	0.06	0.10	2.81	2.86

[a] LOI measured by TG analysis at 950°C.

Table 2
Physical properties of aggregates.

Aggregate	Sand 0–4 mm	Coarse 2–8 mm	Coarse 8–16 mm
Specific gravity	2.65	2.64	2.67
Water absorption (%)	0.33	0.65	0.55

provided by PQ Corporation. The activator solutions were prepared by dissolving sodium hydroxide and sodium silicate in tap water 1 day before mixing.

River sand and gravel were used as the aggregate to prepare the concrete mixtures. Their physical properties including specific gravity and water absorption are summarized in Table 2, and they were air-dried before producing AAC.

2.2. Mixture proportions

In this study, 52 groups of AAC mixtures were investigated. As shown in Table 3, 7 design parameters were presented to describe the mixture proportions of AAC, which will be later converted into predictor variables to build up the RF model. It is noteworthy that the parameters selected here are independent, and as much less relevant as possible from each other. Other parameters, partially repeated, or can be calculated from existing candidates (e.g. the water to binder ratio is determined from the mass ratio between total water content and solid binders) were not considered, and this will be further illustrated in Section 3.1.

From the mix design point of view, multiple design factors have been varied within a certain range to evaluate their effects on the fresh properties and strength development of AACs. Aggregates from 0 to 4, 2–8, and 8–16 mm fractions were applied, and the packing was designed to reach between A16 and B16 curves indicated in DIN 1045–2 among all mixtures. The air content in AAC was estimated to be 1% [28]. Ranges of design parameters in AAC mixture proportions assessed in this study are summarized in Table 3. More details regarding the concrete mixture proportions and statistics of each design parameter are provided in the appendix (Table 8 and Fig. 11).

The concrete mixtures were prepared by a Gustav Eirich SKG1 planetary mixture. Solid precursor and aggregates were first dry-blended for 2 min. Afterwards, the activator solution was gradually added into the mixer (in 30 s), while the mixing was continued for another 3 min ever since the wetting of solid components to derive the fresh AAC mixtures.

2.3. Fresh properties and strength of AACs

The fresh properties of AACs were characterized by slump and rheological parameters as a function of time, which were determined at 5, 20, 35, 50, and 65 min after the first contact between solid ingredients and the liquid alkaline activators, respectively. Slump tests were conducted with an Abrams cone according to EN 12350–2. The rheological behavior of AACs was measured with an ICAR Plus rheometer fitted with a 4-blade vane (130 mm diameter and 130 mm height). For each test, about 20 L of fresh concrete was filled into a cylindrical container (390 mm height and 286 mm inner diameter). The rheometer vane was then inserted into the fresh concrete mixture to perform stress growth and flow curve tests. The static yield stress was expressed as the maximum shear stress reached during the 1-min stress growth test, while the dynamic rheological parameters (dynamic yield stress and plastic viscosity) were obtained through the Reiner-Riwlin equation [29] by applying Bingham model to ramp-down flow curves. After each group test, the concrete was recollected and left at rest until the next testing age, during which a plastic sheet was applied to prevent moist evaporation. In addition, a 1-min remixing was carried out on the concrete mixtures before each group of tests [30].

AAC after tests on fresh properties was cast into 100 mm^3 cubes to determine the compressive strength. Hardened concrete samples were demolded after 24 h and sealed in plastic bags, and they were cured in the moist chamber (20°C with 95% relative humidity) until the target age. Compressive strength tests were conducted at 1, 7, 28, and 91 days according to EN 12390–3. The compressive strength is presented as the average value of 3 replicate samples.

Tests on the fresh and hardened properties of AAC were performed on the same batches of mixtures. However, due to the rapid loss of workability, it was no longer possible to test the fresh properties at later ages in several mixtures. Thereby, in total 193 pieces of compressive strength data and 145 pieces of fresh property data (in terms of slump value, static yield stress, dynamic yield stress, and plastic viscosity) were collected to establish the RF model in this study. Data structures are presented in Table 4. In addition, two groups of mixtures were prepared to validate the properties of the AAC mix design obtained through the grid search optimization.

Table 3
Ranges of design parameters in AAC mixture proportions assessed in this study.

Data set	Precursor content	BFS ratio	Na_2O content	Ms	Water content	Fine aggregate	Coarse aggregate
Unit	kg/m^3	%	kg/m^3	–	kg/m^3	kg/m^3	kg/m^3
Min	320	50	8.04	0	151	630	944
Max	488	100	21.33	1.25	195	755	1131

Table 4
Data structures of AAC fresh and hardened properties assessed in this study.

Data set	Curing age for strength test	Testing age for fresh properties	Compressive strength	Slump	Static yield stress	Dynamic yield stress	Plastic viscosity
Unit	Days	Minutes	MPa	mm	Pa	Pa	Pa·s
Min	1	5	0.3	5	114.1	6.2	37.3
Max	91	65	75.9	275	8442.9	1046.5	372.9

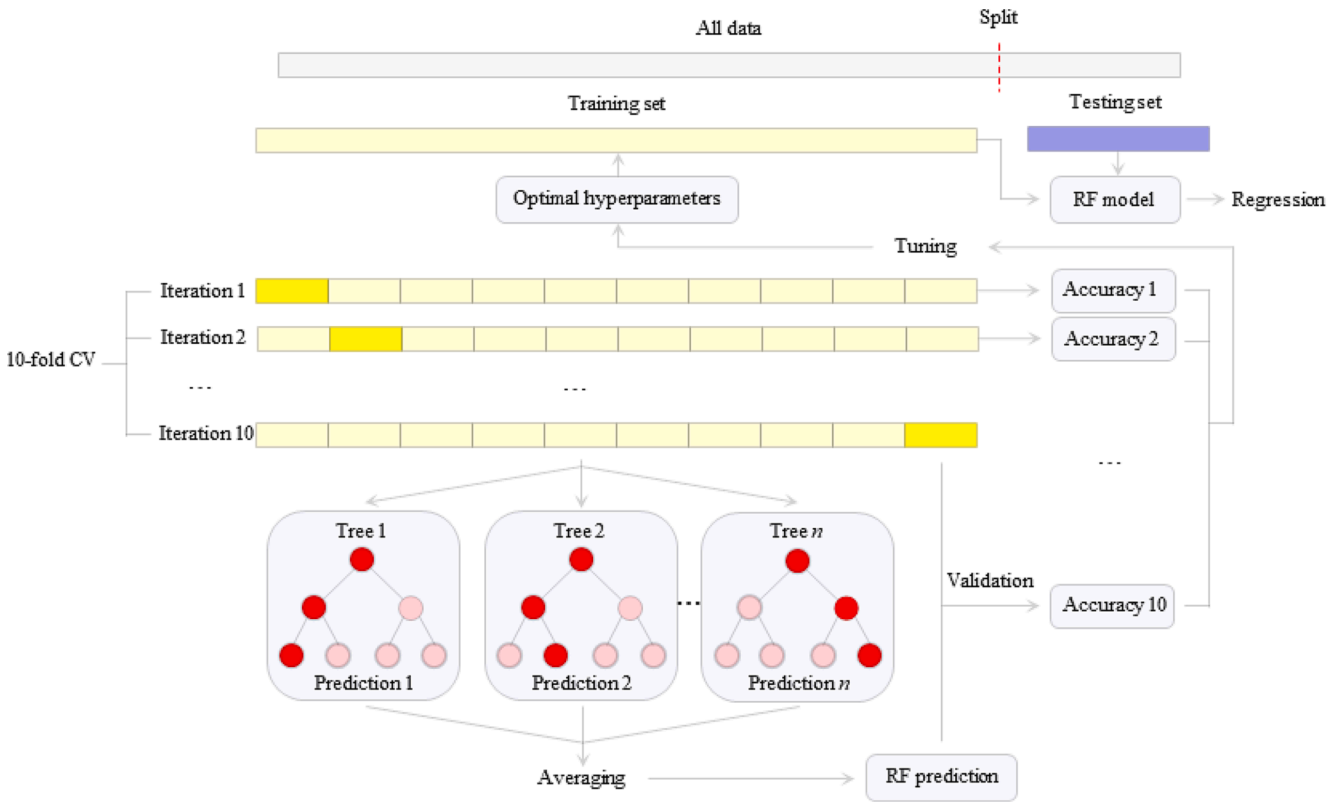

Fig. 3. Diagram of workflows to establish the RF model.

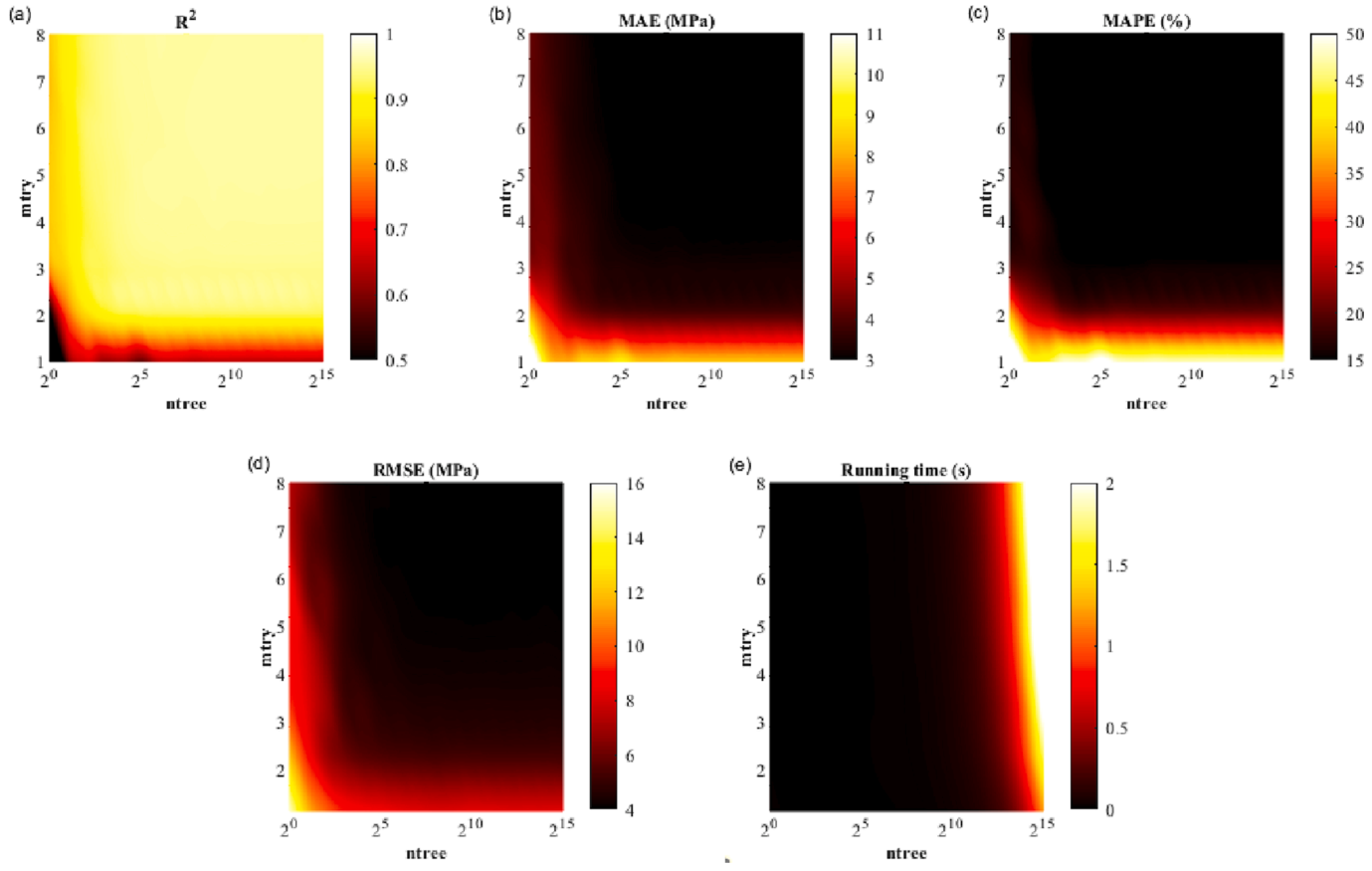

Fig. 4. Hyperparameter tuning for RF model to predict the compressive strength. (a) R^2; (b) MAE; (c) MAPE; (d) RMSE; (e) Running time.

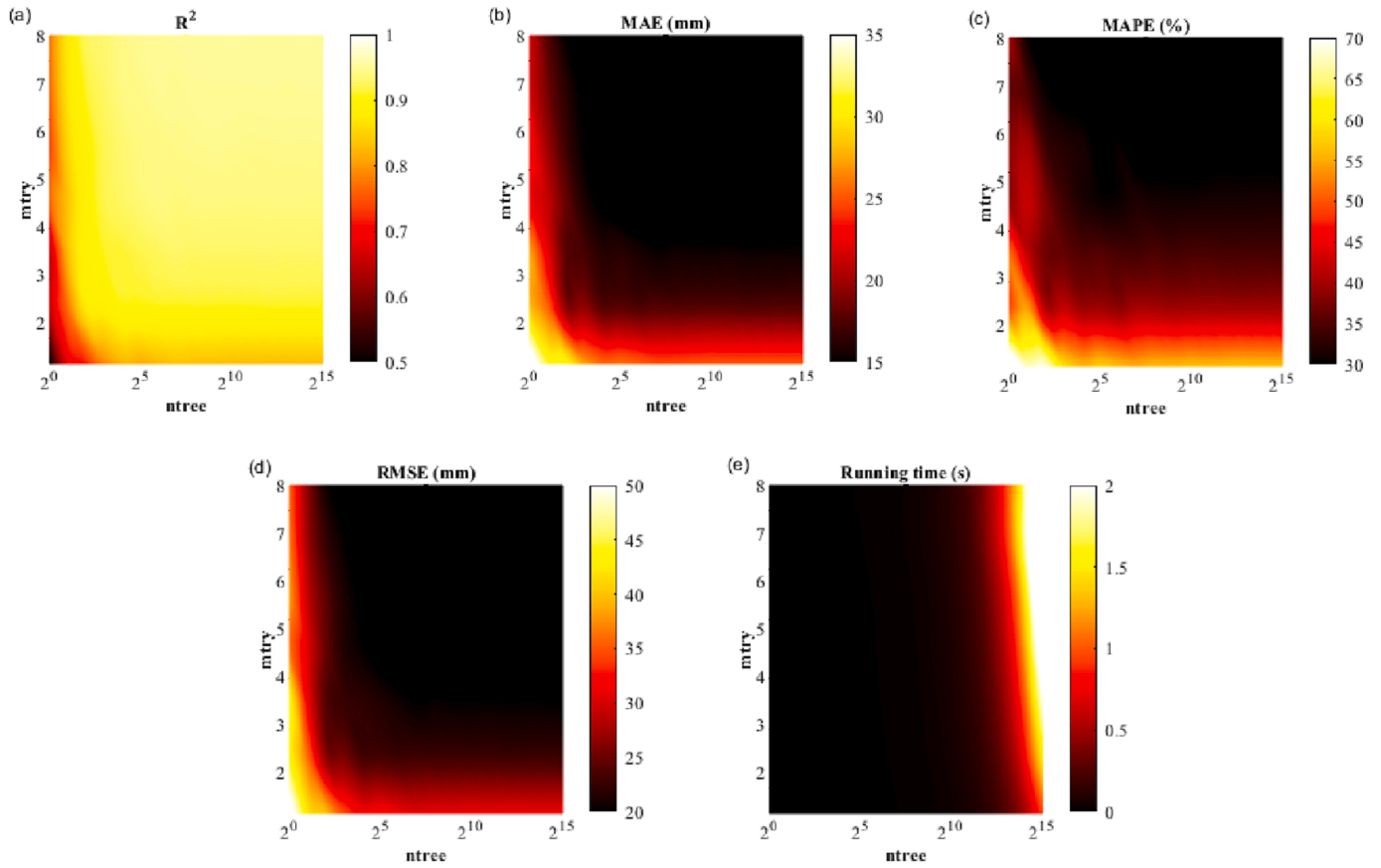

Fig. 5. Hyperparameter tuning for RF model to predict fresh properties (represented by slump predictions). (a) R^2; (b) MAE; (c) MAPE; (d) RMSE; (e) Running time.

2.4. Machine learning model

Random forest is an ensemble machine learning algorithm with a well-known high accuracy in classification and regression [31]. This algorithm consists of several decision trees (DT) that are constructed based on the randomly selected subsets using bootstrap aggregating (bagging) [32], which takes advantage to mitigate the overfitting problems compared with other ML approaches [31]. Considering the regression problems to be solved in this study, the classification and regression tree (CART), which adopts Gini coefficients to evaluate the impurity, is used as the single decision tree in the forest [33]. The randomness of the RF algorithm origins from the following aspects: 1) randomly selecting samples while training single DT, and 2) randomly selecting features while node splitting. By repeating the above steps, the RF model can be constructed based on training sets, and the output of the regression RF is the average value of predictions from each DT, as shown in Fig. 3.

To develop the RF model, results of compressive strength and fresh properties derived from experiments were randomly divided into training and testing datasets, consisting of 80% and 20% data, respectively. The commonly applied 80%/20% split for training and testing sets [34,35] allows the model to be trained in a large enough dataset, while its predictive performance is validated through the remaining testing data, which is hidden from the training process. To ensure the reliability of the regressor and error estimation [36], 10-fold cross-validation [37,38] was applied so that the contribution from each single data point is considered through successive iterations [39], as schematically illustrated in Fig. 3.

3. Results and discussions

3.1. Hyperparameters tuning

The RF algorithm contains several hyperparameters, which will influence the structure and performance of the RF model [40,41]. In this study, two hyperparameters, *mtry* and *ntree*, were tuned to reach an optimal compromise between the predictive performance and computational cost.

The RF algorithm defines *mtry* as the number of drawn candidate variables in each split [42]. In many RF packages, *mtry* is set to $p^{1/2}$ for classification and $p/3$ for regression as default values [40], where p is the number of predictor variables. Lower *mtry* values not only save computational time [43], but also result in less correlated trees with better robusticity while aggregating [40]. However, an optimal *mtry* value might be strongly affected by the degree of correlation among predictor variables. Considering a large *mtry* with many relevant predictor variables, the less influential variables could be 'masked' by stronger candidates and seldomly contribute to the prediction [44]. Instead, *mtry* should be set high if the variables are less relevant [45], so that more influencing factors are considered while constructing the decision tree. Therefore, as announced in previous paragraphs, less relevant design parameters were selected to describe the mixture proportions of AACs, ensuring the simplicity and efficiency of the RF model. On the other hand, *ntree* indicates the number of trees to grow in the forest. It's been suggested that *ntree* should be set sufficiently high [46,47], and more trees always give better predictive performance [48]. In the case of less correlated predictor variables, more trees are expected to build up precise predictions for each observation and obtain good convergence [41]. However, there is also a trade-off between accuracy and computational time, which should be taken into consideration while tuning this hyperparameter.

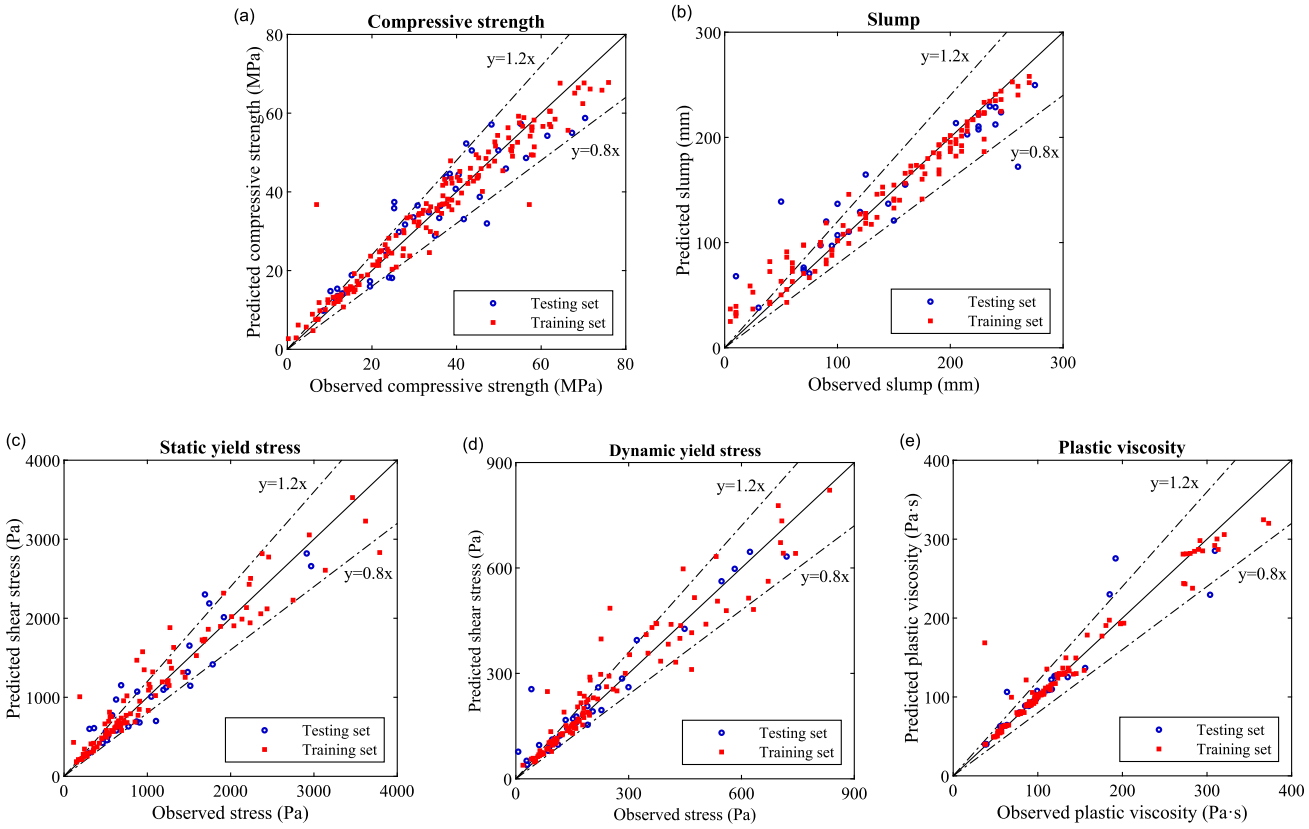

Fig. 6. Regression plot of predicted versus observed values. (a) Compressive strength; (b) Slump; (c) Static yield stress; (d) Dynamic yield stress; (e) Plastic viscosity. (Note: a 20% bound of "y = x" is represented by the dashed lines.).

Table 5
Statistical metrics of RF models.

Statistical metrics		R^2	MAE	MAPE	RMSE
Compressive strength	Training set	0.96	2.45 MPa	9.21%	3.22 MPa
	Testing set	0.92	4.48 MPa	15.98%	5.43 MPa
Slump	Training set	0.93	11.92 mm	26.59%	16.18 mm
	Testing set	0.89	19.11 mm	31.16%	23.88 mm
Static yield stress	Training set	0.92	188.11 Pa	16.53%	285.65 Pa
	Testing set	0.90	184.36 Pa	25.95%	268.93 Pa
Dynamic yield stress	Training set	0.93	38.80 Pa	20.56%	68.81 Pa
	Testing set	0.91	37.00 Pa	20.21%	66.10 Pa
Plastic viscosity	Training set	0.95	7.58 Pa·s	7.43%	17.09 Pa·s
	Testing set	0.94	9.96 Pa·s	6.12%	17.12 Pa·s

Given the number of input design parameters in the AAC dataset, *mtry* was set to range between 1 and 8 (the age of concrete to be tested is also considered here). While an exponential sweep was performed on *ntree*, which was varied from 2^0 to 2^{15}. Grid search optimization [49,50] was employed for the tuning process, through which both hyperparameters were assessed in pairs until an optimal combination.

Statistical metrics were applied to evaluate the predictive performance of RF models, including the coefficient of determination (R^2), mean absolute error (*MAE*), mean absolute percentage error (*MAPE*), and root mean square error (*RMSE*) [51,52,27] as follows:

$$R^2 = 1 - \frac{\sum_{i=1}^{m}(Y_i - \widehat{Y}_i)^2}{\sum_{i=1}^{m}(Y_i - \overline{Y})^2} \tag{1}$$

$$MAE = \frac{1}{m}\sum_{i=1}^{m}|Y_i - \widehat{Y}_i| \tag{2}$$

$$MAPE = \frac{1}{m}\sum_{i=1}^{m}\left|\frac{Y_i - \widehat{Y}_i}{Y_i}\right| \times 100 \tag{3}$$

$$RMSE = \sqrt{\frac{1}{m}\sum_{i=1}^{m}(Y_i - \widehat{Y}_i)^2} \tag{4}$$

where:
m is the size of the dataset,
Y_i is the individual observed value,
$\widehat{Y}_i$ is the predicted output,
$\overline{Y}$ is the mean value of the dataset.

R^2 quantitively describes the accuracy of the predictive model along with the variations of the observed values. An R^2 close to 1 indicates the predictions fit well with the observed data. *MAE* and *RMSE* are defined as parameters to assess the predictive performance in terms of error accumulation, while *MAPE* represents the relative error between predicted and observed values. Thereby smaller *MAE*, *MAPE*, and *RMSE* values suggest a better predictive performance. Apart from that, the running time of each model was also counted to evaluate the computational cost, considering future applications based on an enlarging database.

Statistical metrics obtained by varying the hyperparameters are presented in Fig. 4 and Fig. 5, with similar results in the strength and slump datasets. It is indicated that more accurate predictions were obtained with increases in both *mtry* and *ntree* parameters. However, while

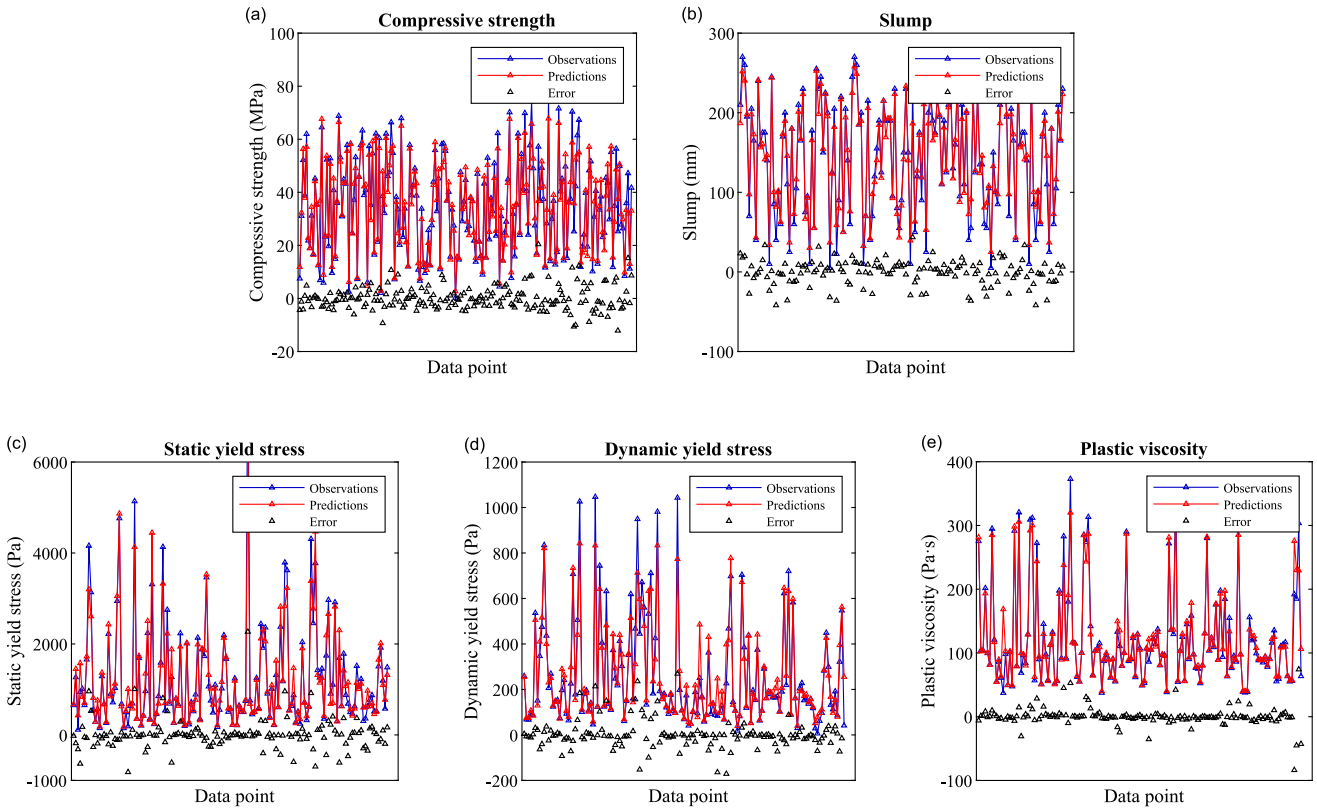

Fig. 7. Predictive performance of the RF model. (a) Compressive strength; (b) Slump; (c) Static yield stress; (d) Dynamic yield stress; (e) Plastic viscosity.

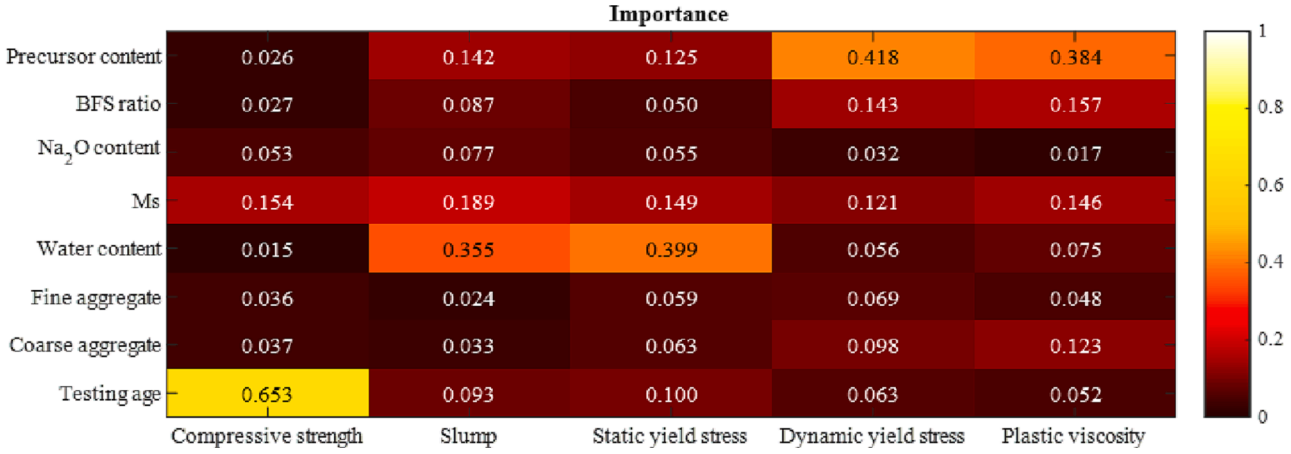

Fig. 8. Importance of predictor variables in RF models. (Note: the importance of each variable is reported as a normalized value of unitless scores).

further increasing *ntree* values above 2^{10}, all statistical metrics maintained relatively stable but a steep increase in running time occurred. Therefore, an optimal hyperparameter set with *mtry* = 8 and *ntree* = 2^{10} was applied in this study considering both the accuracy and computational cost.

3.2. Performance of the RF model

By applying hyperparameters determined from the previous chapter, five RF models were trained for compressive strength, slump, static/dynamic yield stresses, and plastic viscosity predictions. Afterwards, the predictive models were further validated with the testing dataset. It is noteworthy that overfitting and underfitting should be avoided in a practical model [53,54]. The former issue appears when the model fits the training data set so well that it has memorized the noise and the peculiarities of the training data, thus cannot reflect the underlying relationships of the testing set. On the contrary, underfitting refers to a model which is too simple and insufficient to capture the trend in both training and testing sets.

The predictive results of each model, including both training and testing sets, are shown in Fig. 6. It is observed that the vast majority of predictions are fallen into a ± 20% error band deviated from experimental results (y = x), indicating a promising predictive performance. Furthermore, the data points of training and testing sets are mainly distributed in the error band, without severe gathering or scattering, which suggests that no obvious underfitting or overfitting occurred in the predictive models.

Statistical metrics of RF each model are summarized in Table 5. The

Table 6
Ms optimization on AAC mixtures.

Mix	Precursor		Activator		Water (kg/m^3) [c]	Aggregate (kg/m^3) [d]		Optimized Ms [e]			
	Precursor content (kg/m^3)	BFS ratio [a]	Na_2O (kg/m^3)	Ms [b]		Fine	Coarse	Target 1 [f]	Target 2 [g]	Target 3 [h]	Optimal Ms [i]
Opt1	365	100%	10.94	1.25	176	726	1089	N.A.	0.7	0.5	N.A.
Opt2	357	100%	17.86	0.75	176	726	1089	0.4	0.5	0.1	0.5
Opt3	380	100%	15.19	0.75	164	733	1099	0	0.4	N.A.	N.A.
Opt4	367	100%	11.01	1	176	726	1089	N.A.	0.9	0.5	N.A.
Opt5	363	100%	14.52	0.75	176	726	1089	0.2	0.6	0.3	0.6

[a] Defined as the mass proportion of BFS in precursors
[b] Defined as the molar ratio between SiO_2 and Na_2O in the activator
[c] Including the water content in aqueous sodium silicate and the extra water added
[d] The aggregate packing was designed to reach between A16 and B16 curves indicated in DIN 1045–2
[e] Optimized Ms derived from grid search optimization on RF models
[f] Target 1: 1-day compressive strength > 10 MPa
[g] Target 2: 28-day compressive strength > 50 MPa
[h] Target 3: S4 + Slump class (>160 mm)
[i] Defined as minimum Ms which can meet all targets defined in the AACs
N.A. = not applicable, which means the target cannot be achieved throughout the Ms range used in this study.

Table 7
Fresh and hardened properties of optimized AACs.

Mix	Compressive strength (MPa)				Initial slump (mm) Target: 160	
	1-day Target: 10		28-day Target: 50			
	Original	Optimized	Original	Optimized	Original	Optimized
Opt2	24.8	23.8	60.4	54.4	225	215
Opt5	11.8	10.1	57.8	53.5	260	205

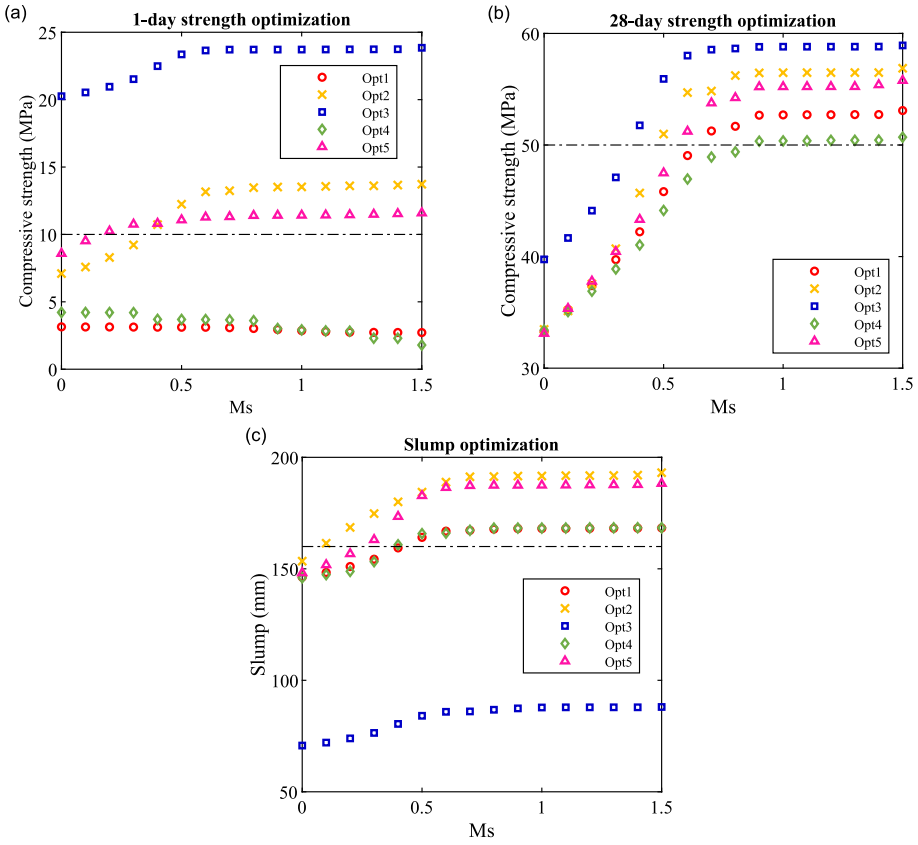

Fig. 9. Grid search optimization on Ms through RF models. (a) 1-day compressive strength; (b) 28-day compressive strength; (c) Slump values.

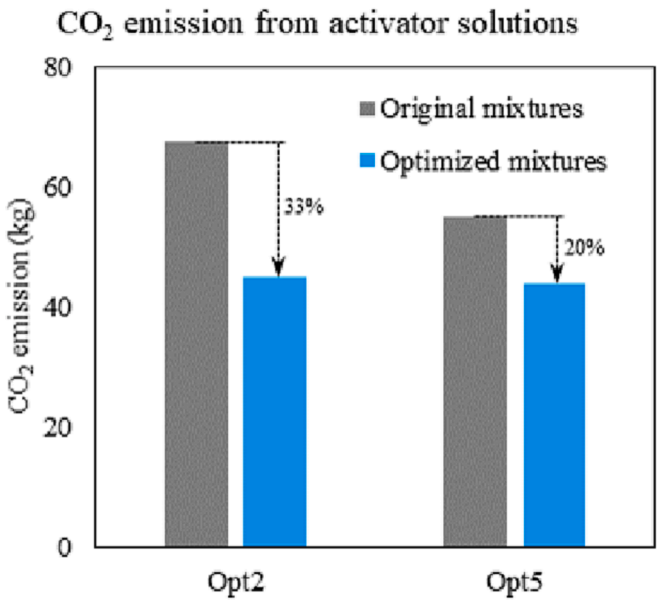

Fig. 10. CO_2 emission from activator solutions for producing per cubic meter AAC.

R^2 values of predictive models were determined as 0.96, 0.93, 0.92, 0.93, and 0.95 in the training set, while slightly dropped to 0.92, 0.89, 0.90, 0.91, and 0.94 by using the testing set, respectively. Similar trends have been detected in other statistical parameters in terms of *MAE*, *MAPE*, and *RMSE*. The results denote a good fitting between the observation and predictions. It is indicated that the RF models established in the current study, in particular the strength predictions, are able to provide equivalent or even superior performance as compared to the existing models developed for PC concrete [13,14,15,16,17] and AAC [27,20,21,22,23] based on AI algorithms.

However, predictions of the fresh properties exhibited less accuracy than those of the compressive strength, which is attributed to the inherent complexity [27]. The fresh property was determined from AAC under dynamic flowing states, which is extremely complicated due to colloidal interactions, Brownian motions, multi-body hydrodynamic interactions, and temporal/spatial correlation of particle positions in a flow field [55,56]. The various interactions are strongly affected by the properties of multiple phases involved in the system, for example, the chemical reactivity of precursors [57], the shape of aggregates [58,59,60], the viscosity of activator solutions [61,62], and the amount of liquid available to fill interstitial spaces [63], etc. Moreover, these interactions are evolving very rapidly due to the strong early reactivities in an AAC system [64,65]. Further, the slump test was manually conducted including the compacting and lifting operations, which might bring uncertainties to the initial flow conditions. For instance, the speed at which the cone was lifted can introduce different kinetic energy to the mixture, leading to different flow conditions and sample shapes at stoppage [66]. Thereby, slightly lower accuracy was detected in slump values as compared to the other predictive models. On the other hand, strength data were determined from hardened AACs, where different particles are tightly packed in a stable matrix with fixed spatial arrangements. At this stage, the microstructure evolution in AACs slowly progressed with dynamic equilibrium in chemical reactions [67], resulting in smaller errors in compressive strength.

It has been observed that all testing sets yielded slight reductions in accuracy as compared to those derived from training sets. The results imply that the predictive models obtained might be less robust while being exposed to a fresh dataset. It might be attributed to the fact that the sample size is not big enough, and the observations used for training are insufficient to capture the trends in a few specific mix design cases. In addition, current predictor variables might be unable to cover all influential factors to achieve more accurate predictions [27]. For instance, previous studies have suggested that the temperature effects [68,69,70], as well as the mixing energy applied [64,71], may lead to a certain impact on both rheology and strength development in AACs. However, such parameters were not considered as key factors in an AAC mix design, thereby excluded from predictor variables in the present models to ensure efficiency and simplicity. Nevertheless, the issues of RF models enumerated above could be gradually resolved with an enlarging database, which covers not only performances of AACs with more variations in mixture proportions, but also predictor variables that better express the influential factors. Accordingly, more follow-up work is expected as a supplement to the current models.

As presented in Fig. 7, the predicted values are plotted against the observed data to assess the global performance of the AAC predictive models. The results reveal that all models showed good accuracy of predictions that the relative errors between predictions and observations are distributed around 0.

3.3. Importance of features

The importance of predictor variables was assessed through mean decrease accuracy computed from permuting out-of-bag (OOB) data in the RF algorithm [31,72]. Normalized importance factors are plotted in the heatmap as present in Fig. 8, where the features with a stronger effect are indicated with light colors. Regarding the compressive strength of AACs, the greatest influence comes from the testing age, in agreement with the results reported by Zhang et al [21]. Apart from that, Ms ranked the top among all AAC design factors, due to the numerous nucleation sites provided by the sodium silicate in the pore solution, which is directly correlated to denser microstructures and higher strength in AACs [73,74]. Slump and static yield stress, which are associated with the initiation of flow from a static state, showed very similar distributions of importance. In both cases, the water content and Ms took the first and second places, respectively. The interstitial water and silicate content may provide fluidizing effects to disperse the solid grains [75,71], thus the interparticle interactions are reduced and less energy is required to initiate the flow. Finally, the rheological conditions to maintain a steady flow are described by dynamic yield stress and plastic viscosity, where the precursor content has the most significant impact. According to the film thickness theory [76], the paste fraction fills the interparticle voids and provides a coating layer on individual aggregates to lubricate the concrete mix. Thereby the interactions induced by precursor grains in the paste are predominant under flowing states. Besides, all the rest variables showed less decisive correlations to the dynamic rheological parameters, with the BFS ratio slightly higher than the others. It is indicated that FA as a substitute material for BFS in this study somewhat improved the dynamic flow of AACs through ball-bearing effects [77].

3.4. Inverse application: Mix optimization

As is well-known that AAC is developed as an alternative green concrete, with lower carbon footprints than PC materials [78,79,80]. It is remarkable that this statement is sometimes controversial since the usage of highly concentrated alkaline activators in AACs on the other hand causes another significant environmental impact, depending on the type and dosage of activators applied though. Sodium silicate is one of the most commonly used alkaline activators to promote the activation reaction, which benefits AACs in both fresh and hardened states [71,73]. However, its manufacturing process is associated with heavy energy consumption and CO_2 emission because of the high temperature and pressure required [79,81]. Due to the lack of standardized design regulations, it might be the case that some AAC mixtures are over-designed by using an excessive amount of sodium silicate while exceeding the practical demands. Therefore, this study further attempts to optimize

Table 8
Mixture proportions and compressive strength data of AAM concretes tested in this study.

Data point	Precursor		Activator		Water (kg/m^3) [c]	Aggregate (kg/m^3) [d]	Curing time (day)	Compressive strength (MPa)
	Precursor content (kg/m^3)	BFS ratio [a]	NaOH (kg/m^3)	Ms [b]				
1	375	100%	15.00	0.45	153	1822	1	28.9
2	375	100%	15.00	0.45	153	1822	7	42.7
3	375	100%	15.00	0.45	153	1822	28	62.0
4	375	100%	15.00	0.45	153	1822	91	70.2
5	375	100%	19.34	0	151	1819	1	15.2
6	375	100%	19.34	0	151	1819	7	23.9
7	375	100%	19.34	0	151	1819	28	36.2
8	375	100%	19.34	0	151	1819	91	40.6
9	386	100%	17.42	0.25	164	1832	1	15.8
10	386	100%	17.42	0.25	164	1832	7	32.8
11	386	100%	17.42	0.25	164	1832	28	45.2
12	386	100%	17.42	0.25	164	1832	91	53.0
13	354	100%	15.97	0.25	187	1800	1	9.6
14	354	100%	15.97	0.25	187	1800	7	21.8
15	354	100%	15.97	0.25	187	1800	28	31.9
16	354	100%	15.97	0.25	187	1800	91	37.6
17	383	100%	14.81	0.5	164	1832	1	24.7
18	383	100%	14.81	0.5	164	1832	7	43.3
19	383	100%	14.81	0.5	164	1832	28	63.3
20	383	100%	14.81	0.5	164	1832	91	64.5
21	350	100%	13.57	0.5	187	1800	1	14.3
22	350	100%	13.57	0.5	187	1800	7	28.3
23	350	100%	13.57	0.5	187	1800	28	37.5
24	350	100%	13.57	0.5	187	1800	91	38.6
25	380	100%	12.25	0.75	164	1832	1	27.3
26	380	100%	12.25	0.75	164	1832	7	58.1
27	380	100%	12.25	0.75	164	1832	28	70.4
28	380	100%	12.25	0.75	164	1832	91	75.9
29	363	100%	11.71	0.75	176	1815	1	11.8
30	363	100%	11.71	0.75	176	1815	7	44.9
31	363	100%	11.71	0.75	176	1815	28	57.8
32	363	100%	11.71	0.75	176	1815	91	62.1
33	348	100%	11.22	0.75	187	1800	1	9.6
34	348	100%	11.22	0.75	187	1800	7	36.0
35	348	100%	11.22	0.75	187	1800	28	47.0
36	348	100%	11.22	0.75	187	1800	91	54.4
37	374	100%	12.66	0.25	176	1815	1	12.4
38	374	100%	12.66	0.25	176	1815	7	23.6
39	374	100%	12.66	0.25	176	1815	28	33.5
40	374	100%	12.66	0.25	176	1815	91	38.9
41	371	100%	10.78	0.5	176	1815	1	13.2
42	371	100%	10.78	0.5	176	1815	7	25.3
43	371	100%	10.78	0.5	176	1815	28	37.2
44	371	100%	10.78	0.5	176	1815	91	42.3
45	369	100%	8.93	0.75	176	1815	1	6.1
46	369	100%	8.93	0.75	176	1815	7	32.8
47	369	100%	8.93	0.75	176	1815	28	45.2
48	369	100%	8.93	0.75	176	1815	91	52.3
49	367	100%	7.10	1	176	1815	1	2.1
50	367	100%	7.10	1	176	1815	7	37.9
51	367	100%	7.10	1	176	1815	28	53.1
52	367	100%	7.10	1	176	1815	91	61.5
53	365	100%	5.29	1.25	176	1815	1	0.2
54	365	100%	5.29	1.25	176	1815	7	41.2
55	365	100%	5.29	1.25	176	1815	28	57.4
56	365	100%	5.29	1.25	176	1815	91	67.3
57	363	100%	11.71	0.75	176	1815	1	11.8
58	363	100%	11.71	0.75	176	1815	7	44.9
59	363	100%	11.71	0.75	176	1815	28	57.8
60	363	100%	11.71	0.75	176	1815	91	62.1
61	361	100%	17.45	0.5	176	1815	1	19.5
62	361	100%	17.45	0.5	176	1815	7	36.8
63	361	100%	17.45	0.5	176	1815	28	47.5
64	361	100%	17.45	0.5	176	1815	91	55.9
65	357	100%	14.40	0.75	176	1815	1	24.8
66	357	100%	14.40	0.75	176	1815	7	50.9
67	357	100%	14.40	0.75	176	1815	28	60.4
68	357	100%	14.40	0.75	176	1815	91	67.9
69	356	100%	20.64	0.5	176	1815	1	24.0
70	356	100%	20.64	0.5	176	1815	7	39.8
71	356	100%	20.64	0.5	176	1815	28	52.8
72	356	100%	20.64	0.5	176	1815	91	62.1
73	369	100%	16.66	0.25	176	1815	1	12.5

(*continued on next page*)

Table 8 (*continued*)

Data point	Precursor		Activator		Water (kg/m^3) [c]	Aggregate (kg/m^3) [d]	Curing time (day)	Compressive strength (MPa)
	Precursor content (kg/m^3)	BFS ratio [a]	NaOH (kg/m^3)	Ms [b]				
74	369	100%	16.66	0.25	176	1815	7	27.4
75	369	100%	16.66	0.25	176	1815	28	38.9
76	369	100%	16.66	0.25	176	1815	91	44.0
77	369	90%	16.66	0.25	176	1815	1	12.0
78	369	90%	16.66	0.25	176	1815	7	21.8
79	369	90%	16.66	0.25	176	1815	28	30.9
80	369	90%	16.66	0.25	176	1815	91	37.7
81	369	80%	16.66	0.25	176	1815	1	11.0
82	369	80%	16.66	0.25	176	1815	7	21.4
83	369	80%	16.66	0.25	176	1815	28	27.6
84	369	80%	16.66	0.25	176	1815	91	35.3
85	369	60%	16.66	0.25	176	1815	1	7.3
86	369	60%	16.66	0.25	176	1815	7	16.5
87	369	60%	16.66	0.25	176	1815	28	23.1
88	369	60%	16.66	0.25	176	1815	91	27.5
89	366	100%	14.17	0.5	176	1815	1	19.5
90	366	100%	14.17	0.5	176	1815	7	33.9
91	366	100%	14.17	0.5	176	1815	28	45.8
92	366	100%	14.17	0.5	176	1815	91	48.3
93	366	90%	14.17	0.5	176	1815	1	14.6
94	366	90%	14.17	0.5	176	1815	7	40.3
95	366	90%	14.17	0.5	176	1815	28	51.7
96	366	90%	14.17	0.5	176	1815	91	62.3
97	366	80%	14.17	0.5	176	1815	1	10.2
98	366	80%	14.17	0.5	176	1815	7	30.8
99	366	80%	14.17	0.5	176	1815	28	40.5
100	366	80%	14.17	0.5	176	1815	91	49.1
101	366	60%	14.17	0.5	176	1815	1	9.0
102	366	60%	14.17	0.5	176	1815	7	29.1
103	366	60%	14.17	0.5	176	1815	28	38.8
104	366	60%	14.17	0.5	176	1815	91	44.6
105	400	100%	20.65	0	160	1811	1	15.7
106	400	100%	20.65	0	160	1811	7	22.2
107	400	100%	20.65	0	160	1811	28	32.2
108	400	100%	20.65	0	160	1811	91	43.2
109	450	100%	23.23	0	180	1710	1	13.1
110	450	100%	23.23	0	180	1710	7	19.7
111	450	100%	23.23	0	180	1710	28	33.5
112	450	100%	23.23	0	180	1710	91	38.4
113	487.5	100%	25.16	0	195	1634	1	16.0
114	487.5	100%	25.16	0	195	1634	7	23.1
115	487.5	100%	25.16	0	195	1634	28	31.0
116	487.5	100%	25.16	0	195	1634	91	40.2
117	320	100%	14.06	0.5	160	1886	1	23.3
118	320	100%	14.06	0.5	160	1886	7	49.0
119	320	100%	14.06	0.5	160	1886	28	52.2
120	320	100%	14.06	0.5	160	1886	91	71.6
121	360	100%	15.82	0.5	180	1794	1	24.7
122	360	100%	15.82	0.5	180	1794	7	45.5
123	360	100%	15.82	0.5	180	1794	28	43.6
124	360	100%	15.82	0.5	180	1794	91	68.8
125	390	100%	17.14	0.5	195	1726	1	25.8
126	390	100%	17.14	0.5	195	1726	7	46.1
127	390	100%	17.14	0.5	195	1726	28	53.2
128	390	100%	17.14	0.5	195	1726	91	74.4
129	400	100%	17.58	0.5	160	1808	1	16.8
130	400	100%	17.58	0.5	160	1808	7	31.2
131	400	100%	17.58	0.5	160	1808	28	40.8
132	400	100%	17.58	0.5	160	1808	91	54.7
133	450	100%	19.77	0.5	180	1706	1	17.0
134	450	100%	19.77	0.5	180	1706	7	29.8
135	450	100%	19.77	0.5	180	1706	28	40.8
136	450	100%	19.77	0.5	180	1706	91	55.2
137	487.5	100%	21.42	0.5	195	1630	1	19.0
138	487.5	100%	21.42	0.5	195	1630	7	31.1
139	487.5	100%	21.42	0.5	195	1630	28	36.7
140	487.5	100%	21.42	0.5	195	1630	91	55.6
141	400	100%	19.11	0.25	160	1809	1	12.8
142	400	100%	19.11	0.25	160	1809	7	33.8
143	400	100%	19.11	0.25	160	1809	91	58.4
144	450	100%	21.50	0.25	180	1708	1	14.3
145	450	100%	21.50	0.25	180	1708	7	35.2
146	450	100%	21.50	0.25	180	1708	91	57.7
147	487.5	100%	23.29	0.25	195	1632	1	11.8

(*continued on next page*)

Table 8 (*continued*)

Data point	Precursor		Activator		Water (kg/m^3) [c]	Aggregate (kg/m^3) [d]	Curing time (day)	Compressive strength (MPa)
	Precursor content (kg/m^3)	BFS ratio [a]	NaOH (kg/m^3)	Ms [b]				
148	487.5	100%	23.29	0.25	195	1632	7	34.9
149	487.5	100%	23.29	0.25	195	1632	91	56.4
150	400	100%	8.79	0.5	160	1822	1	2.6
151	400	100%	8.79	0.5	160	1822	7	25.3
152	400	100%	8.79	0.5	160	1822	91	49.7
153	450	100%	9.89	0.5	180	1722	1	4.5
154	450	100%	9.89	0.5	180	1722	7	25.7
155	450	100%	9.89	0.5	180	1722	91	49.2
156	487.5	100%	10.71	0.5	195	1648	1	5.9
157	487.5	100%	10.71	0.5	195	1648	7	24.0
158	487.5	100%	10.71	0.5	195	1648	91	49.9
159	400	50%	20.65	0	160	1764	1	6.7
160	400	50%	20.65	0	160	1764	7	14.9
161	400	50%	20.65	0	160	1764	91	30.0
162	450	50%	23.23	0	180	1658	1	7.2
163	450	50%	23.23	0	180	1658	7	15.5
164	450	50%	23.23	0	180	1658	91	27.8
165	487.5	50%	25.16	0	195	1577	1	7.5
166	487.5	50%	25.16	0	195	1577	7	13.8
167	487.5	50%	25.16	0	195	1577	91	26.4
168	400	50%	17.58	0.5	160	1761	1	8.5
169	400	50%	17.58	0.5	160	1761	7	35.5
170	400	50%	17.58	0.5	160	1761	28	47.6
171	400	50%	17.58	0.5	160	1761	91	58.3
172	450	50%	19.77	0.5	180	1654	1	7.7
173	450	50%	19.77	0.5	180	1654	7	35.9
174	450	50%	19.77	0.5	180	1654	28	45.1
175	450	50%	19.77	0.5	180	1654	91	57.8
176	487.5	50%	21.42	0.5	195	1574	91	6.9
177	487.5	50%	21.42	0.5	195	1574	1	33.6
178	487.5	50%	21.42	0.5	195	1574	7	47.2
179	487.5	50%	21.42	0.5	195	1574	91	57.2
180	400	75%	20.65	0	160	1788	1	11.2
181	400	75%	20.65	0	160	1788	7	20.2
182	400	75%	20.65	0	160	1788	91	38.9
183	450	75%	23.23	0	180	1684	1	11.6
184	450	75%	23.23	0	180	1684	7	21.1
185	450	75%	23.23	0	180	1684	91	36.8
186	487.5	75%	25.16	0	195	1606	1	10.8
187	487.5	75%	25.16	0	195	1606	7	21.6
188	487.5	75%	25.16	0	195	1606	91	36.6
189	400	75%	17.58	0.5	160	1785	1	14.0
190	400	75%	17.58	0.5	160	1785	7	38.2
191	400	75%	17.58	0.5	160	1785	91	69.8
192	450	75%	19.77	0.5	180	1680	1	15.4
193	450	75%	19.77	0.5	180	1680	7	36.5

[a] Defined as the mass proportion of BFS in precursors

[b] Defined as the mass ratio between SiO_2 and Na_2O in the activator

[c] Including the water content in aqueous sodium silicate and the extra water added

[d] Including the particle fractions of 0–4, 2–8, and 8–16 mm, with a mass ratio of 1:0.69:0.81. The aggregate packing was designed to reach between A16 and B16 curves indicated in DIN 1045–2.

AAC mix designs with lower environmental impact, which is achieved by reducing the sodium silicate dosage as much as possible while meeting the target strength and slump values. An optimal Ms is derived through the grid search optimization on established RF models, until the lowest Ms meeting all target predictions occurred.

To showcase the optimization process, five mixtures with the highest sodium silicate dosages per cubic meter of AAC were selected from the database, as listed in Table 6, where Ms was defined as the optimization objective. Three explicit targets have been made, as an example here, that the AAC was expected to achieve 10 MPa 1-day strength, 50 MPa 28-day strength, and the initial slump should reach S4 class (>160 mm according to EN 206). Further, they were set as threshold values to assess the grid search optimization results, as indicated by the dashed lines in Fig. 9.

As shown in Fig. 9 (a), a declined 1-day strength in Opt1 and Opt4 with higher Ms has been captured by the strength predictive model. However, it has been observed that neither of them achieved the target throughout the Ms range used in this study. This is attributed to their low sodium concentration and high Ms in the original mixtures. Both factors may slow down the dissolution of precursors [4,82–84], while high Ms further results in a long induction period, thereby inhibiting the early-strength development [85,86]. On the contrary, this target could be achieved with lower Ms values in the other mixtures, where the high Na_2O content ensures a more rapid strength development at early ages. Moreover, the results indicate that higher slump and 28-day strength values could be obtained by increasing the silicate dosage in alkaline activators. This is in agreement with and can be well-explained by the previous studies on the effect of sodium silicates [71,73].

The minimum Ms which fulfills all designated targets was determined as the optimal value, as indicated in Table 6, which can potentially reduce the sodium silicate content in AAC mixtures. The strength and slump values of optimized mixtures with reduced Ms were further validated by trial mixes. It is noticed that the maximum slump that might be achieved with Ms traverse in Opt4 was less than 100 mm, and it was then excluded from the optimization set in addition to Opt1 and Opt3. Eventually, it was determined to reduce the silicate dosage in

Table 9
Mixture proportions and fresh properties data of AAM concretes tested in this study.

Data point	Precursor		Activator		Water (kg/m^3) [c]	Aggregate (kg/m^3) [d]	Testing age (min)	Slump (mm)	Static yield stress (Pa)	Dynamic yield stress (Pa)	Plastic viscosity (Pa·s)
	Precursor content (kg/m^3)	BFS ratio [a]	NaOH (kg/m^3)	Ms [b]							
1	375	100%	15.00	0.45	153	1822	5	175	943.24	164.12	129.49
2	375	100%	15.00	0.45	153	1822	20	125	1315.95	190.22	122.69
3	375	100%	15.00	0.45	153	1822	35	90	1743.38	181.83	132.32
4	375	100%	15.00	0.45	153	1822	50	80	2239.17	196.64	125.31
5	375	100%	15.00	0.45	153	1822	65	75	2966.29	197.75	137.10
6	375	100%	19.34	0	151	1819	5	70	3311.05	361.97	180.50
7	375	100%	19.34	0	151	1819	20	60	3775.43	374.47	197.72
8	375	100%	19.34	0	151	1819	35	40	4762.77	475.02	197.62
9	375	100%	19.34	0	151	1819	50	10	8442.93	948.90	201.69
10	386	100%	17.42	0.25	164	1832	5	10	5137.19	622.52	309.09
11	354	100%	15.97	0.25	187	1800	5	190	507.33	128.09	55.20
12	354	100%	15.97	0.25	187	1800	20	175	643.52	173.38	52.43
13	354	100%	15.97	0.25	187	1800	35	145	756.31	219.09	55.23
14	354	100%	15.97	0.25	187	1800	50	110	906.38	247.57	56.45
15	354	100%	15.97	0.25	187	1800	65	40	1103.81	290.93	57.58
16	383	100%	14.81	0.5	164	1832	5	60	2378.39	532.70	285.24
17	383	100%	14.81	0.5	164	1832	20	25	2912.92	720.04	294.84
18	383	100%	14.81	0.5	164	1832	35	5	4306.58	1046.50	309.32
19	350	100%	13.57	0.5	187	1800	5	240	261.40	68.78	49.60
20	350	100%	13.57	0.5	187	1800	20	225	282.67	88.99	47.52
21	350	100%	13.57	0.5	187	1800	35	205	303.22	97.12	48.98
22	350	100%	13.57	0.5	187	1800	50	190	350.60	106.80	51.51
23	350	100%	13.57	0.5	187	1800	65	165	354.03	101.13	52.28
24	380	100%	12.25	0.75	164	1832	5	95	1691.35	444.90	271.74
25	380	100%	12.25	0.75	164	1832	20	75	1914.51	581.99	275.41
26	380	100%	12.25	0.75	164	1832	35	55	2456.19	697.82	280.10
27	380	100%	12.25	0.75	164	1832	50	30	2944.04	834.42	290.02
28	380	100%	12.25	0.75	164	1832	65	10	3619.55	981.16	320.38
29	363	100%	11.71	0.75	176	1815	5	200	501.87	106.68	98.00
30	363	100%	11.71	0.75	176	1815	20	160	636.78	124.15	96.52
31	363	100%	11.71	0.75	176	1815	35	125	653.78	136.79	100.25
32	363	100%	11.71	0.75	176	1815	50	100	680.54	157.26	103.93
33	363	100%	11.71	0.75	176	1815	65	85	718.57	161.20	103.34
34	348	100%	11.22	0.75	187	1800	5	260	172.15	30.09	39.13
35	348	100%	11.22	0.75	187	1800	20	240	197.49	48.71	37.50
36	348	100%	11.22	0.75	187	1800	35	225	218.64	52.96	37.78
37	348	100%	11.22	0.75	187	1800	50	200	236.71	58.23	38.92
38	348	100%	11.22	0.75	187	1800	65	185	263.92	60.70	38.45
39	374	100%	12.66	0.25	176	1815	5	95	1289.34	346.71	129.53
40	374	100%	12.66	0.25	176	1815	20	70	1784.57	438.33	135.91
41	374	100%	12.66	0.25	176	1815	35	10	2361.46	670.99	156.00
42	371	100%	10.78	0.5	176	1815	5	105	1033.52	153.74	119.70
43	371	100%	10.78	0.5	176	1815	20	95	1240.58	168.82	121.43
44	371	100%	10.78	0.5	176	1815	35	55	1672.74	195.35	123.29
45	371	100%	10.78	0.5	176	1815	50	40	1878.46	204.40	129.36
46	371	100%	10.78	0.5	176	1815	65	25	2135.90	227.58	130.85
47	369	100%	8.93	0.75	176	1815	5	150	754.62	120.73	101.03
48	369	100%	8.93	0.75	176	1815	20	135	878.51	146.49	98.18
49	369	100%	8.93	0.75	176	1815	35	90	1064.59	164.52	103.56
50	369	100%	8.93	0.75	176	1815	50	70	1267.21	176.49	106.78
51	369	100%	8.93	0.75	176	1815	65	50	1589.00	190.52	99.29
52	367	100%	7.10	1	176	1815	5	210	507.59	95.33	90.14
53	367	100%	7.10	1	176	1815	20	160	634.71	137.45	95.28
54	367	100%	7.10	1	176	1815	35	155	687.59	149.38	87.56
55	367	100%	7.10	1	176	1815	50	150	797.68	151.92	90.11
56	367	100%	7.10	1	176	1815	65	130	902.54	160.78	88.49
57	365	100%	5.29	1.25	176	1815	5	190	685.37	92.96	92.38
58	365	100%	5.29	1.25	176	1815	20	135	1020.33	140.10	86.12
59	365	100%	5.29	1.25	176	1815	35	120	1179.24	153.19	89.38
60	365	100%	5.29	1.25	176	1815	50	110	1249.65	180.89	85.02
61	365	100%	5.29	1.25	176	1815	65	100	1454.27	195.85	86.28
62	363	100%	11.71	0.75	176	1815	5	200	501.87	106.68	98.00
63	363	100%	11.71	0.75	176	1815	20	160	680.54	124.15	96.52
64	363	100%	11.71	0.75	176	1815	35	125	718.57	136.79	100.25
65	363	100%	11.71	0.75	176	1815	50	100	636.78	157.26	103.93
66	363	100%	11.71	0.75	176	1815	65	85	653.78	161.20	103.34
67	361	100%	17.45	0.5	176	1815	5	215	422.44	63.82	90.24
68	361	100%	17.45	0.5	176	1815	20	200	457.92	108.94	97.65
69	361	100%	17.45	0.5	176	1815	35	190	496.40	109.86	93.97
70	361	100%	17.45	0.5	176	1815	50	170	500.62	117.30	90.06
71	361	100%	17.45	0.5	176	1815	65	160	607.52	118.87	96.92
72	357	100%	14.40	0.75	176	1815	5	225	354.61	18.78	80.69

(*continued on next page*)

Table 9 (*continued*)

Data point	Precursor		Activator		Water (kg/m^3) [c]	Aggregate (kg/m^3) [d]	Testing age (min)	Slump (mm)	Static yield stress (Pa)	Dynamic yield stress (Pa)	Plastic viscosity (Pa·s)
	Precursor content (kg/m^3)	BFS ratio [a]	NaOH (kg/m^3)	Ms [b]							
73	357	100%	14.40	0.75	176	1815	20	210	452.06	28.55	78.26
74	357	100%	14.40	0.75	176	1815	35	195	519.22	41.03	75.21
75	357	100%	14.40	0.75	176	1815	50	180	569.96	74.22	80.54
76	357	100%	14.40	0.75	176	1815	65	175	676.06	94.91	81.71
77	356	100%	20.64	0.5	176	1815	5	245	245.35	6.25	89.59
78	356	100%	20.64	0.5	176	1815	20	225	463.87	61.80	90.23
79	356	100%	20.64	0.5	176	1815	35	220	511.13	88.09	87.19
80	356	100%	20.64	0.5	176	1815	50	210	543.66	96.41	91.83
81	356	100%	20.64	0.5	176	1815	65	205	627.88	105.87	91.27
82	369	100%	16.66	0.25	176	1815	5	110	1014.24	241.05	116.04
83	369	100%	16.66	0.25	176	1815	20	85	1515.49	385.00	123.67
84	369	100%	16.66	0.25	176	1815	35	60	2038.99	467.56	135.33
85	369	100%	16.66	0.25	176	1815	50	5	2749.57	631.92	145.38
86	369	90%	16.66	0.25	176	1815	5	150	714.63	191.79	109.03
87	369	90%	16.66	0.25	176	1815	20	125	1047.45	282.39	112.36
88	369	90%	16.66	0.25	176	1815	35	95	1657.91	351.33	115.24
89	369	90%	16.66	0.25	176	1815	50	50	2010.98	448.71	116.69
90	369	90%	16.66	0.25	176	1815	65	10	2436.87	505.38	120.75
91	369	80%	16.66	0.25	176	1815	5	190	552.67	133.16	96.34
92	369	80%	16.66	0.25	176	1815	20	177.5	746.25	178.65	99.68
93	369	80%	16.66	0.25	176	1815	35	140	1098.02	217.53	107.08
94	369	80%	16.66	0.25	176	1815	50	120	1225.65	268.85	107.48
95	369	80%	16.66	0.25	176	1815	65	90	1424.64	299.47	105.29
96	369	60%	16.66	0.25	176	1815	5	245	305.01	92.79	61.13
97	369	60%	16.66	0.25	176	1815	20	230	360.14	132.29	56.98
98	369	60%	16.66	0.25	176	1815	35	220	490.74	180.78	55.40
99	369	60%	16.66	0.25	176	1815	50	215	568.44	187.81	59.32
100	369	60%	16.66	0.25	176	1815	65	190	624.97	206.02	61.03
101	366	100%	14.17	0.5	176	1815	5	175	690.48	112.17	110.74
102	366	100%	14.17	0.5	176	1815	20	140	773.00	144.79	115.18
103	366	100%	14.17	0.5	176	1815	35	100	871.47	159.65	113.42
104	366	100%	14.17	0.5	176	1815	50	70	888.24	177.62	114.06
105	366	100%	14.17	0.5	176	1815	65	55	1011.13	190.99	116.59
106	366	90%	14.17	0.5	176	1815	5	240	323.28	86.92	76.18
107	366	90%	14.17	0.5	176	1815	20	225	513.93	92.33	76.54
108	366	90%	14.17	0.5	176	1815	35	215	524.70	100.95	79.50
109	366	90%	14.17	0.5	176	1815	50	210	590.48	123.38	83.92
110	366	90%	14.17	0.5	176	1815	65	200	618.99	150.86	79.85
111	366	80%	14.17	0.5	176	1815	5	260	204.65	66.85	63.29
112	366	80%	14.17	0.5	176	1815	20	245	212.74	81.92	62.51
113	366	80%	14.17	0.5	176	1815	35	235	278.58	86.95	65.63
114	366	80%	14.17	0.5	176	1815	50	225	323.43	97.93	63.46
115	366	80%	14.17	0.5	176	1815	65	215	396.57	103.79	61.90
116	366	60%	14.17	0.5	176	1815	5	270	147.43	45.83	55.74
117	366	60%	14.17	0.5	176	1815	20	255	148.85	62.92	55.16
118	366	60%	14.17	0.5	176	1815	35	240	215.93	67.65	54.61
119	366	60%	14.17	0.5	176	1815	50	235	230.19	68.13	55.20
120	366	60%	14.17	0.5	176	1815	65	230	356.68	85.88	56.11
121	450	100%	23.23	0	180	1710	5	60	3136.38	711.27	191.91
122	487.5	100%	25.16	0	195	1634	5	105	2190.03	536.20	184.94
123	320	100%	14.06	0.5	160	1886	5	150	1505.49	425.06	141.95
124	360	100%	15.82	0.5	180	1794	5	230	852.11	467.29	52.97
125	390	100%	17.14	0.5	195	1726	5	260	188.61	83.92	37.28
126	400	100%	17.58	0.5	160	1808	5	120	4157.40	1042.94	366.77
127	450	100%	19.77	0.5	180	1706	5	205	1731.26	321.60	372.88
128	487.5	100%	21.42	0.5	195	1630	5	230	962.08	169.73	274.00
129	400	100%	19.11	0.25	160	1809	5	22.5	3463.26	707.30	291.69
130	450	100%	21.50	0.25	180	1708	5	55	1918.70	372.45	311.77
131	487.5	100%	23.29	0.25	195	1632	5	90	1690.79	225.56	272.31
132	450	100%	9.89	0.5	180	1722	5	50	3789.39	618.89	313.26
133	487.5	100%	10.71	0.5	195	1648	5	110	2233.50	436.24	303.65
134	400	50%	20.65	0	160	1764	5	70	2222.55	703.86	144.96
135	450	50%	23.23	0	180	1658	5	195	1192.81	547.01	93.64
136	487.5	50%	25.16	0	195	1577	5	205	545.89	226.64	68.86
137	400	50%	17.58	0.5	160	1761	5	230	873.56	412.71	184.56
138	450	50%	19.77	0.5	180	1654	5	270	577.26	302.45	86.22
139	487.5	50%	21.42	0.5	195	1574	5	275	114.12	41.28	63.58
140	400	75%	20.65	0	160	1788	5	40	4131.87	1026.10	158.41
141	450	75%	23.23	0	180	1684	5	125	1484.57	743.83	133.21
142	487.5	75%	25.16	0	195	1606	5	165	1261.67	559.68	154.81
143	400	75%	17.58	0.5	160	1785	5	150	1271.30	250.23	282.88
144	450	75%	19.77	0.5	180	1680	5	230	908.02	405.32	175.82
145	487.5	75%	21.42	0.5	195	1602	5	245	535.50	258.97	110.70

[a] Defined as the mass proportion of BFS in precursors
[b] Defined as the mass ratio between SiO_2 and Na_2O in the activator
[c] Including the water content in aqueous sodium silicate and the extra water added
[d] Including the particle fractions of 0–4, 2–8, and 8–16 mm, with a mass ratio of 1:0.69:0.81. The aggregate packing was designed to reach between A16 and B16 curves indicated in DIN 1045–2.

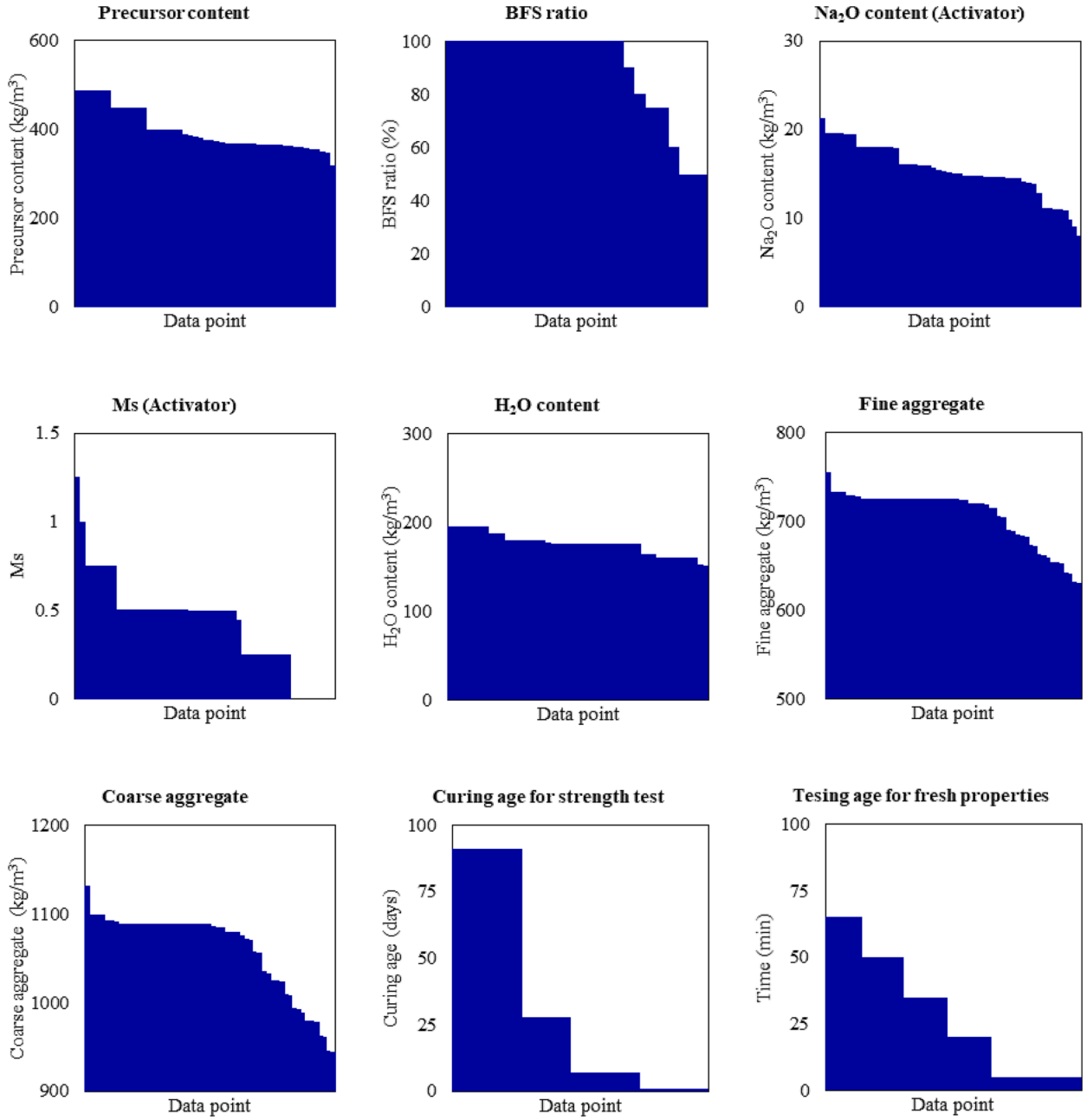

Fig. 11. Statistics of AAC mixtures in this study.

Opt2 and Opt5, while the slight variations per unit volume of AAC were compensated by the aggregate content. Finally, the optimized mixtures were produced to assess their actual performances.

As presented in Table 7, all optimized AAC mixtures have exceeded the pre-defined demands in both slump and strength values. Nevertheless, it's been observed in all models that the predictive performance of AACs tends to reach a plateau in high Ms ranges. It is likely that their properties are correlated to multiple design factors, while further increases in Ms may not improve the strength and workability. The most reasonable explanation would be that the observed data with higher Ms values involved in this study is limited, since the excessive silicate in the activators resulted in very rapid workability loss of AACs (i.e. the 'flash setting' occurred) [64] in trial mixes. Thereby, more data is expected to improve the RF models towards making more precise predictions in this region.

In general, the results illustrate that a proper design in Ms may contribute to the reduction in environmental impacts induced by AACs. With specified demands, the optimization process provides the possibility to mitigate the overdesign in terms of high silicate dosages. According to the relevant emissions reported in [87], as shown in Fig. 10, it

is expected that the optimized mix design saves approximately 33% and 20% of CO_2 from the activator phases for producing per cubic meter of Opt2 and Opt5, respectively. It can be deduced that the mixture optimization approach present in this study is capable of future applications to produce 'greener' AACs by using an appropriate sodium silicate dosage.

3.5. Discussions and future perspectives

Due to the limited raw materials involved in this study, concerns might arise that the RF model developed is only capable of local applications. It is expected that the current model could be progressively optimized with more supplementary results from various AAC mixtures. However, the data collecting work is struggling in the current situation, due to the absence of commonly applied design codes and parameters in AACs. Data conversion has to be done at first while comparing or integrating the results from different literature, and sometimes the key information is unfortunately missing by using different expressions to describe the mix design.

In PC systems, the binder is classified into different cement types, where the inherent material properties (e.g. composition, reactivity, grinding fineness, etc.) are revealed by the strength development features in standard mixtures. By contrast, the classification system of AAM binders is still underdeveloped, which is once again ascribed to the diversity in raw materials and complexity of reaction mechanisms. In many studies, solid activators are considered as part of the binder in AAMs [28], and the effect of binder chemistry on activation reactions has been thoroughly elaborated [88,89,90,4,91]. A few recent research further well progressed to establish a composition-performance relationship in AAMs by analyzing the big data collected from literature [21,20]. Apart from that, however, it should be noticed that the reactivity in AACs could be affected by other factors such as the amorphous content and particle fineness of precursors, as well as the complex interactions between various precursors and activators. Hence, a systematic classification of AAM binders is in urgent demand to assist global data integrations from the literature with locally available raw materials, which promotes the development of more reliable predictive models and design codes. In view of the application of PC and one-part AAMs ('just add water' like PC materials) [91], the classification could be potentially achieved by assessing combinations of precursors and activators in standard mixtures.

The AI concrete mix optimization based on ML algorithms has attracted attention in recent years [92], which saves laboratory works from trial mixes as compared to the conventional optimization approach. With the development of multi-objective optimization algorithms [93], the variations in concrete performances in terms of strength, workability, cost, carbon footprint, etc. could be more easily evaluated [94]. This study further provided an inverse single-objective mix optimization on AACs through grid searching, which gives the optimal predictor variables by specifying demands of concrete performance. However, it might be time-consuming and even unrealistic to provide global mix design optimizations simultaneously with multiple design parameters in a complex AAC system by using grid search. This issue might be solved with more advanced multi-objective optimization algorithms [95], which could be potentially applied as an AAC mix design tool to inversely output design parameters based on a reliable predictive model. More relevant research in the field is expected to facilitate the development of AI concrete mix design and optimization approaches.

4. Conclusions

This study dedicates to establishing random forest (RF) predictive models for the strength and fresh properties of alkali-activated concrete (AAC), which is made of blast furnace slag (BFS) and coal fly ash (FA). From laboratory tests, 193 compressive strength data and 145 workability data (in terms of slump, static/dynamic yield stress, and plastic viscosity) were collected for training and validation. Results show that the performance of AACs could be well-predicted with equivalent or even superior accuracy as compared to other predictive models based on machine learning algorithms. Multiple mix design parameters were assessed through the importance analysis integrated with the model. The compressive strength is indicated to be most relevant to the curing age and silicate modulus (Ms) applied, while the water content is predominant in slump values and static yield stress of AACs.

Furthermore, an inverse single-objective optimization in Ms has been conducted based on the RF models obtained, as the sodium silicate in activators is one of the primary sources of CO_2 emissions in AACs. With specified workability and strength demands, a minimum Ms meeting all target values is derived through optimization. The results indicate that the environmental impact of AACs could be further reduced with an appropriate silicate dosage obtained from the mix optimization approach proposed. However, multi-objective optimization of AAC design parameters is still problematic. A comprehensive AAC mix design tool can be expected with the development of more advanced multi-objective optimization algorithms and reliable predictive models.

CRediT authorship contribution statement

Yubo Sun: Conceptualization, Methodology, Investigation, Writing – original draft. **Hao Cheng:** Methodology, Investigation, Writing – original draft. **Shizhe Zhang:** Methodology, Writing – review & editing. **Manu K. Mohan:** Methodology, Writing – review & editing. **Guang Ye:** Supervision, Writing – review & editing. **Geert De Schutter:** Funding acquisition, Supervision, Writing – review & editing.

Declaration of Competing Interest

The authors declare that they have no known competing financial interests or personal relationships that could have appeared to influence the work reported in this paper.

Data availability

Data will be made available on request.

Acknowledgement

This paper presents the research results from the DuRSAAM project. The financial support from the European Union's Horizon 2020 research and innovation programme (ETN DuRSAAM – H2020-MSCA-ITN-2018-813596) is gratefully acknowledged.

Appendix

References

[1] P.-C. Aïtcin, Cements of yesterday and today: concrete of tomorrow, Cem. Concr. Res. 30 (2000) 1349–1359.
[2] K.L. Scrivener, Options for the future of cement, Indian Concr. J. 88 (2014) 11–21.
[3] A. Herrmann, A. Koenig, F. Dehn, Structural concrete based on alkali-activated binders: Terminology, reaction mechanisms, mix designs and performance, Struct. Concr. 19 (2018) 918–929, https://doi.org/10.1002/suco.201700016.
[4] P. Duxson, J.L. Provis, Designing precursors for geopolymer cements, J. Am. Ceram. Soc. 91 (2008) 3864–3869, https://doi.org/10.1111/j.1551-2916.2008.02787.x.
[5] S.R. Gislason, E.H. Oelkers, Mechanism, rates, and consequences of basaltic glass dissolution: II. An experimental study of the dissolution rates of basaltic glass as a function of pH and temperature, Geochim. Cosmochim. Acta 67 (2003) 3817–3832.
[6] J.L. Provis, J.S.J. Van Deventer, RILEM State-of-the-Art Reports State-of-the-Art Report, RILEM TC 224-AAM, n.d.

[7] J.L. Provis, A. Palomo, C. Shi, Cement and Concrete Research Advances in understanding alkali-activated materials, Cem. Concr. Res. 78 (2015) 110–125, https://doi.org/10.1016/j.cemconres.2015.04.013.
[8] J.L. Provis, Activating solution chemistry for geopolymers, in: Geopolymers, Elsevier, 2009, pp. 50–71.
[9] J.L. Provis, Geopolymers and other alkali activated materials: Why, how, and what? Mater. Struct. Constr. 47 (2014) 11–25, https://doi.org/10.1617/s11527-013-0211-5.
[10] S.A. Bernal, J.L. Provis, A. Fernández-jiménez, P.V. Krivenko, E. Kavalerova, M. Palacios, C. Shi, Alkali Activated Materials (2014). http://link.springer.com/10.1007/978-94-007-7672-2.
[11] R.S. Michalski, J.G. Carbonell, T.M. Mitchell, Machine learning: An artificial intelligence approach, Springer Science & Business Media, 2013.
[12] G.F. Luger, Artificial intelligence: structures and strategies for complex problem solving, Pearson education, 2005.
[13] S. Lai, M. Serra, Concrete strength prediction by means of neural network, Constr. Build. Mater. 11 (1997) 93–98.
[14] D.-C. Feng, Z.-T. Liu, X.-D. Wang, Y. Chen, J.-Q. Chang, D.-F. Wei, Z.-M. Jiang, Machine learning-based compressive strength prediction for concrete: An adaptive boosting approach, Constr. Build. Mater. 230 (2020), 117000.
[15] J. Duan, P.G. Asteris, H. Nguyen, X.-N. Bui, H. Moayedi, A novel artificial intelligence technique to predict compressive strength of recycled aggregate concrete using ICA-XGBoost model, Eng. Comput. 37 (2021) 3329–3346.
[16] J.-S. Chou, A.-D. Pham, Enhanced artificial intelligence for ensemble approach to predicting high performance concrete compressive strength, Constr. Build. Mater. 49 (2013) 554–563.
[17] M.-Y. Cheng, J.-S. Chou, A.F.V. Roy, Y.-W. Wu, High-performance concrete compressive strength prediction using time-weighted evolutionary fuzzy support vector machines inference model, Autom. Constr. 28 (2012) 106–115.
[18] R. Nogueira, A. Silva, A. Silva, Prediction of strength and heterogeneity of low-strength mortars from drilling data, Constr. Build. Mater. 305 (2021), 124738.
[19] B. Baten, T. Manzur, T. Torsha, S. Alam, A parametric study on the graphical approach to assess corrosion vulnerability of concrete mixes in chloride environment, Constr. Build. Mater. 309 (2021), 125115.
[20] X. Ke, Y. Duan, Coupling machine learning with thermodynamic modelling to develop a composition-property model for alkali-activated materials, Compos. B Eng. 216 (2021), 108801, https://doi.org/10.1016/j.compositesb.2021.108801.
[21] L.V. Zhang, A. Marani, M.L. Nehdi, Chemistry-informed machine learning prediction of compressive strength for alkali-activated materials, Constr. Build. Mater. 316 (2022), 126103, https://doi.org/10.1016/j.conbuildmat.2021.126103.
[22] D. Van Dao, H.B. Ly, S.H. Trinh, T.T. Le, B.T. Pham, Artificial intelligence approaches for prediction of compressive strength of geopolymer concrete, Materials (Basel). 12 (2019), https://doi.org/10.3390/ma12060983.
[23] K.T. Nguyen, Q.D. Nguyen, T.A. Le, J. Shin, K. Lee, Analyzing the compressive strength of green fly ash based geopolymer concrete using experiment and machine learning approaches, Constr. Build. Mater. 247 (2020), 118581.
[24] K.K. Ramagiri, S.P. Boindala, M. Zaid, A. Kar, Random Forest-Based Algorithms for Prediction of Compressive Strength of Ambient-Cured AAB Concrete—A Comparison Study, in: Proc. SECON'21 Struct. Eng. Constr. Manag., Springer, 2022: pp. 717–725.
[25] V. Toufigh, A. Jafari, Developing a comprehensive prediction model for compressive strength of fly ash-based geopolymer concrete (FAGC), Constr. Build. Mater. 277 (2021), 122241.
[26] Y. Peng, C. Unluer, Analyzing the mechanical performance of fly ash-based geopolymer concrete with different machine learning techniques, Constr. Build. Mater. 316 (2022), 125785.
[27] E. Gomaa, T. Han, M. ElGawady, J. Huang, A. Kumar, Machine learning to predict properties of fresh and hardened alkali-activated concrete, Cem. Concr. Compos. 115 (2021), 103863, https://doi.org/10.1016/j.cemconcomp.2020.103863.
[28] J.L. Provis, K. Arbi, S.A. Bernal, D. Bondar, A. Buchwald, A. Castel, S. Chithiraputhiran, M. Cyr, A. Dehghan, K. Dombrowski-Daube, A. Dubey, V. Ducman, G.J.G. Gluth, S. Nanukuttan, K. Peterson, F. Puertas, A. van Riessen, M. Torres-Carrasco, G. Ye, Y. Zuo, RILEM TC 247-DTA round robin test: mix design and reproducibility of compressive strength of alkali-activated concretes, Mater. Struct. Constr. 52 (2019) 1–13, https://doi.org/10.1617/s11527-019-1396-z.
[29] D. Feys, J.E. Wallevik, A. Yahia, K.H. Khayat, O.H. Wallevik, Extension of the Reiner-Riwlin equation to determine modified Bingham parameters measured in coaxial cylinders rheometers, Mater. Struct. Constr. 46 (2013) 289–311, https://doi.org/10.1617/s11527-012-9902-6.
[30] F. Puertas, B. González-Fonteboa, I. González-Taboada, M.M. Alonso, M. Torres-Carrasco, G. Rojo, F. Martínez-Abella, Alkali-activated slag concrete: Fresh and hardened behaviour, Cem. Concr. Compos. (2018), https://doi.org/10.1016/j.cemconcomp.2017.10.003.
[31] L. Breiman, Random forests, Mach. Learn. 45 (2001) 5–32.
[32] L. Breiman, Bagging predictors, Mach. Learn. 24 (1996) 123–140.
[33] L. Breiman, J.H. Friedman, R.A. Olshen, C.J. Stone, Classification and regression trees, Routledge, 2017.
[34] R.A. Taylor, J.R. Pare, A.K. Venkatesh, H. Mowafi, E.R. Melnick, W. Fleischman, M. K. Hall, Prediction of in-hospital mortality in emergency department patients with sepsis: a local big data–driven, machine learning approach, Acad. Emerg. Med. 23 (2016) 269–278.
[35] N.K. Tran, S. Sen, T.L. Palmieri, K. Lima, S. Falwell, J. Wajda, H.H. Rashidi, Artificial intelligence and machine learning for predicting acute kidney injury in severely burned patients: a proof of concept, Burns 45 (2019) 1350–1358.
[36] S. Varma, R. Simon, Bias in error estimation when using cross-validation for model selection, BMC Bioinf. 7 (2006) 1–8.
[37] S. Yadav S. Shukla Analysis of k-fold cross-validation over hold-out validation on colossal datasets for quality classification, in, IEEE 6th Int. Conf. Adv. Comput IEEE 2016 2016 78 83.
[38] T. Fushiki, Estimation of prediction error by using K-fold cross-validation, Stat. Comput. 21 (2011) 137–146.
[39] P. Refaeilzadeh, L. Tang, H. Liu, Cross-validation, Encycl. Database Syst. 5 (2009) 532–538.
[40] P. Probst, M.N. Wright, A. Boulesteix, Hyperparameters and tuning strategies for random forest, Wiley Interdiscip, Rev. Data Min. Knowl. Discov. 9 (2019) e1301.
[41] P. Schratz, J. Muenchow, E. Iturritxa, J. Richter, A. Brenning, Hyperparameter tuning and performance assessment of statistical and machine-learning algorithms using spatial data, Ecol. Model. 406 (2019) 109–120.
[42] R. Genuer, J.-M. Poggi, C. Tuleau-Malot, Variable selection using random forests, Pattern Recogn. Lett. 31 (2010) 2225–2236.
[43] M.N. Wright, A. Ziegler, ranger: A fast implementation of random forests for high dimensional data in C++ and R, ArXiv Prepr. ArXiv1508.04409 (2015).
[44] S. Bernard, L. Heutte, S. Adam, Influence of hyperparameters on random forest accuracy, in: Int. Work. Mult. Classif. Syst., Springer, 2009: pp. 171–180.
[45] B.A. Goldstein, E.C. Polley, F.B.S. Briggs, Random forests for genetic association studies, Stat. Appl. Genet. Mol. Biol. 10 (2011).
[46] R. Díaz-Uriarte, S. Alvarez de Andrés, Gene selection and classification of microarray data using random forest, BMC Bioinf. 7 (2006) 1–13.
[47] T.M. Oshiro, P.S. Perez, J.A. Baranauskas, How many trees in a random forest?, in: Int. Work. Mach. Learn. Data Min. Pattern Recognit., Springer, 2012: pp. 154–168.
[48] P. Probst, A.-L. Boulesteix, To tune or not to tune the number of trees in random forest, J. Mach. Learn. Res. 18 (2017) 6673–6690.
[49] J. Bergstra, Y. Bengio, Random search for hyper-parameter optimization, J. Mach. Learn. Res. 13 (2012).
[50] P. Liashchynskyi, P. Liashchynskyi, Grid search, random search, genetic algorithm: A big comparison for NAS, ArXiv Prepr. ArXiv1912.06059. (2019).
[51] L. Zhang, M. Su, Y. Wang, Development of the use of sulfo-and ferroaluminate cements in China, Adv. Cem. Res. 11 (1999) 15–21.
[52] H.-G. Ni, J.-Z. Wang, Prediction of compressive strength of concrete by neural networks, Cem. Concr. Res. 30 (2000) 1245–1250.
[53] H. Jabbar, R.Z. Khan, Methods to avoid over-fitting and under-fitting in supervised machine learning (comparative study), Comput. Sci. Commun. Instrum. Devices. 70 (2015).
[54] W.M.P. Van der Aalst, V. Rubin, H.M.W. Verbeek, B.F. van Dongen, E. Kindler, C. W. Günther, Process mining: a two-step approach to balance between underfitting and overfitting, Softw. Syst. Model. 9 (2010) 87–111.
[55] N. Roussel, A. Lemaître, R.J. Flatt, P. Coussot, Steady state flow of cement suspensions: A micromechanical state of the art, Cem. Concr. Res. 40 (2010) 77–84, https://doi.org/10.1016/j.cemconres.2009.08.026.
[56] J. Koelman, P.J. Hoogerbrugge, Dynamic simulations of hard-sphere suspensions under steady shear, EPL (Europhysics Lett. 21 (1993) 363.
[57] A. Kashani, Influence of precursors on rheology of alkali-activated materials, Handb. Adv. Alkali-Activated Concr., Elsevier, in, 2022, pp. 107–124.
[58] J. Hu, K. Wang, Effect of coarse aggregate characteristics on concrete rheology, Constr. Build. Mater. 25 (2011) 1196–1204.
[59] M. Westerholm, B. Lagerblad, J. Silfwerbrand, E. Forssberg, Influence of fine aggregate characteristics on the rheological properties of mortars, Cem. Concr. Compos. 30 (2008) 274–282, https://doi.org/10.1016/j.cemconcomp.2007.08.008.
[60] M.R. Geiker, M. Brandl, L.N. Thrane, L.F. Nielsen, On the effect of coarse aggregate fraction and shape on the rheological properties of self-compacting concrete, Cem. Concr. Aggregates. 24 (2002) 3–6.
[61] M.F. Alnahhal, T. Kim, A. Hajimohammadi, Distinctive rheological and temporal viscoelastic behaviour of alkali-activated fly ash/slag pastes: A comparative study with cement paste, Cem. Concr. Res. 144 (2021), 106441, https://doi.org/10.1016/j.cemconres.2021.106441.
[62] Y. Sun, S. Zhang, A.V. Rahul, Y. Tao, F. Van Bockstaele, K. Dewettinck, G. Ye, G. De Schutter, Rheology of alkali-activated slag pastes: New insight from microstructural investigations by cryo-SEM, Cem. Concr. Res. 157 (2022), 106806, https://doi.org/10.1016/j.cemconres.2022.106806.
[63] C. Leonelli, M. Romagnoli, Rheology parameters of alkali-activated geopolymeric concrete binders, Woodhead Publishing Limited (2015), https://doi.org/10.1533/9781782422884.2.133.
[64] M. Palacios, S. Gismera, M.M. Alonso, J.B. Espinose, D. Lacaillerie, B. Lothenbach, A. Favier, C. Brumaud, F. Puertas, Cement and Concrete Research Early reactivity of sodium silicate-activated slag pastes and its impact on rheological properties, Cem. Concr. Res. 140 (2021), 106302, https://doi.org/10.1016/j.cemconres.2020.106302.
[65] M. Palacios, P.F.G. Banfill, F. Puertas, Rheology and setting of alkali-activated slag pastes and mortars: Effect of organic admixture, ACI Mater. J. 105 (2008) 140.
[66] N. Roussel, C. Stéfani, R. Leroy, From mini-cone test to Abrams cone test: measurement of cement-based materials yield stress using slump tests, Cem. Concr. Res. 35 (2005) 817–822.
[67] R. Cao, S. Zhang, N. Banthia, Y. Zhang, Z. Zhang, Interpreting the early-age reaction process of alkali-activated slag by using combined embedded ultrasonic measurement, thermal analysis, XRD, FTIR and SEM, Compos. B Eng. 186 (2020), 107840, https://doi.org/10.1016/j.compositesb.2020.107840.
[68] M. Palacios, M.M. Alonso, C. Varga, F. Puertas, Influence of the alkaline solution and temperature on the rheology and reactivity of alkali-activated fly ash pastes, Cem. Concr. Compos. 95 (2019) 277–284.

[69] S. Siddique, V. Gupta, S. Chaudhary, S. Park, J.-G. Jang, Influence of the Precursor, Molarity and Temperature on the Rheology and Structural Buildup of Alkali-Activated Materials, Materials (Basel). 14 (2021) 3590.
[70] P. Zhang, Z. Gao, J. Wang, J. Guo, S. Hu, Y. Ling, Properties of fresh and hardened fly ash/slag based geopolymer concrete: A review, J. Clean. Prod. 270 (2020), 122389.
[71] F. Puertas, C. Varga, M.M. Alonso, Rheology of alkali-activated slag pastes. Effect of the nature and concentration of the activating solution, Cem. Concr. Compos. 53 (2014) 279–288, https://doi.org/10.1016/j.cemconcomp.2014.07.012.
[72] A. Boulesteix, S. Janitza, J. Kruppa, I.R. König, Overview of random forest methodology and practical guidance with emphasis on computational biology and bioinformatics, Wiley Interdiscip, Rev. Data Min. Knowl. Discov. 2 (2012) 493–507.
[73] M.H. Hubler, J.J. Thomas, H.M. Jennings, Influence of nucleation seeding on the hydration kinetics and compressive strength of alkali activated slag paste, Cem. Concr. Res. 41 (2011) 842–846, https://doi.org/10.1016/j.cemconres.2011.04.002.
[74] B.S. Gebregziabiher, R. Thomas, S. Peethamparan, Very early-age reaction kinetics and microstructural development in alkali-activated slag, Cem. Concr. Compos. 55 (2015) 91–102, https://doi.org/10.1016/j.cemconcomp.2014.09.001.
[75] Y. Tian, C. Yang, S. Yuan, H. Yuan, K. Yang, L. Yu, M. Zhang, X. Zhu, Understanding the rheological properties of alkali-activated slag pastes from the cohesion and friction interactions, Constr. Build. Mater. 291 (2021), 123311.
[76] L.G. Li, A.K.H. Kwan, Concrete mix design based on water film thickness and paste film thickness, Cem. Concr. Compos. 39 (2013) 33–42.
[77] H. Vikan, H. Justnes, Rheology of cementitious paste with silica fume or limestone, Cem. Concr. Res. 37 (2007) 1512–1517, https://doi.org/10.1016/j.cemconres.2007.08.012.
[78] P. Duxson, D.G. Brice, Chemical Research and Climate Change as Drivers in the Commercial Adoption of Alkali Activated Materials, (2010) 145–155. https://doi.org/10.1007/s12649-010-9015-9.
[79] L.K. Turner, F.G. Collins, Carbon dioxide equivalent (CO2-e) emissions: A comparison between geopolymer and OPC cement concrete, Constr. Build. Mater. 43 (2013) 125–130, https://doi.org/10.1016/j.conbuildmat.2013.01.023.
[80] K.A. Komnitsas, Potential of geopolymer technology towards green buildings and sustainable cities, Procedia Eng. 21 (2011) 1023–1032, https://doi.org/10.1016/j.proeng.2011.11.2108.
[81] B.C. McLellan, R.P. Williams, J. Lay, A. Van Riessen, G.D. Corder, Costs and carbon emissions for geopolymer pastes in comparison to ordinary portland cement, J. Clean. Prod. 19 (2011) 1080–1090.
[82] Y. Zuo, G. Ye, Preliminary interpretation of the induction period in hydration of sodium hydroxide/silicate activated slag, Materials (Basel). 13 (2020) 1–19, https://doi.org/10.3390/ma13214796.
[83] J.-J. Chang, A study on the setting characteristics of sodium silicate-activated slag pastes, Cem. Concr. Res. 33 (2003) 1005–1011.
[84] D. Ravikumar, N. Neithalath, Reaction kinetics in sodium silicate powder and liquid activated slag binders evaluated using isothermal calorimetry, Thermochim Acta 546 (2012) 32–43, https://doi.org/10.1016/j.tca.2012.07.010.
[85] B.S. Gebregziabiher, R.J. Thomas, S. Peethamparan, Temperature and activator effect on early-age reaction kinetics of alkali-activated slag binders, Constr. Build. Mater. 113 (2016) 783–793, https://doi.org/10.1016/j.conbuildmat.2016.03.098.
[86] C. Shi, R.L. Day, A calorimetric study of early hydration of alkali-slag cements, Cem. Concr. Res. 25 (1995) 1333–1346.
[87] X. Dai, S. Aydın, M.Y. Yardımcı, K. Lesage, G. De Schutter, Rheology and microstructure of alkali-activated slag cements produced with silica fume activator, Cem. Concr. Compos. 104303 (2021).
[88] M. Ben Haha, G. Le Saout, F. Winnefeld, B. Lothenbach, Influence of activator type on hydration kinetics, hydrate assemblage and microstructural development of alkali activated blast-furnace slags, Cem. Concr. Res. 41 (2011) 301–310, https://doi.org/10.1016/j.cemconres.2010.11.016.
[89] M. Ben Haha, B. Lothenbach, G. Le Saout, F. Winnefeld, Influence of slag chemistry on the hydration of alkali-activated blast-furnace slag - Part II: Effect of Al2O3, Cem. Concr. Res. 42 (2012) 74–83, https://doi.org/10.1016/j.cemconres.2011.08.005.
[90] M. Ben Haha, B. Lothenbach, G. Le Saout, F. Winnefeld, Influence of slag chemistry on the hydration of alkali-activated blast-furnace slag - Part I: Effect of MgO, Cem. Concr. Res. 41 (2011) 955–963, https://doi.org/10.1016/j.cemconres.2011.05.002.
[91] T. Luukkonen, Z. Abdollahnejad, J. Yliniemi, P. Kinnunen, M. Illikainen, One-part alkali-activated materials: A review, Cem. Concr. Res. 103 (2018) 21–34, https://doi.org/10.1016/j.cemconres.2017.10.001.
[92] M.A. DeRousseau, J.R. Kasprzyk, W.V. Srubar Iii, Computational design optimization of concrete mixtures: A review, Cem. Concr. Res. 109 (2018) 42–53.
[93] K. Miettinen, Nonlinear multiobjective optimization, Springer Science & Business Media, 2012.
[94] J. Zhang, Y. Huang, Y. Wang, G. Ma, Multi-objective optimization of concrete mixture proportions using machine learning and metaheuristic algorithms, Constr. Build. Mater. 253 (2020), 119208, https://doi.org/10.1016/j.conbuildmat.2020.119208.
[95] C. Dong, B. Zeng, Expert learning through generalized inverse multiobjective optimization: Models, insights, and algorithms, in: Int. Conf. Mach. Learn., PMLR, 2020: pp. 2648–2657.